

Distribution Agreement

In presenting this thesis as a partial fulfillment of the requirements for a degree from Emory University, I hereby grant to Emory University and its agents the non-exclusive license to archive, make accessible, and display my thesis in whole or in part in all forms of media, now or hereafter now, including display on the World Wide Web. I understand that I may select some access restrictions as part of the online submission of this thesis. I retain all ownership rights to the copyright of the thesis. I also retain the right to use in future works (such as articles or books) all or part of this thesis.

Thomas Joseph Kowal-Safron

March 17, 2020

Computational and Experimental Studies of Allylic C-H Functionalization of Internal Olefins via
Group IX Metal- π -Allyl Intermediates and Invention of a Chiral Indenylrhodium(III) Catalyst

By

Thomas Joseph Kowal-Safron

Simon B. Blakey

Adviser

Department of Chemistry

Simon B. Blakey

Adviser

Patricia Marsteller

Committee Member

Antonio Brathwaite

Committee Member

Cora E. MacBeth

Committee Member

2020

Computational and Experimental Studies of Allylic C-H Functionalization of Internal Olefins via
Group IX Metal- π -Allyl Intermediates and Invention of a Chiral Indenylrhodium(III) Catalyst

By

Thomas Joseph Kowal-Safron

Simon B. Blakey

Adviser

An abstract of
a thesis submitted to the Faculty of Emory College of Arts and Sciences
of Emory University in partial fulfillment
of the requirements of the degree of
Bachelor of Science with Honors

Department of Chemistry

2020

Abstract

Computational and Experimental Studies of Allylic C-H Functionalization of Internal Olefins via Group IX Metal- π -Allyl Intermediates and Invention of a Chiral Indenylrhodium(III) Catalyst
By Thomas Joseph Kowal-Safron

Transition metal-catalyzed allylic C-H functionalization has found its place on the cutting edge of C-H functionalization due to its vast potential to access allylic C-H bonds for direct modification. Recent advances of this methodology have significant applications in pharmaceutically relevant syntheses for more facile methodologies that will curtail cost and waste generation. Based on the elucidation of reaction conditions that facilitated the regioselective allylic C-H amination of internal olefins by Blakey, it was hypothesized that similar reaction conditions for allylic C-H alkylation with malonate-derivative carbon nucleophiles could be developed. An optimization study was carried out using dimethyl malonate as the nucleophile for the alkylation of 1,3-*trans*-diphenylpropene. The optimal reaction conditions were found to tolerate five malonate-derivative carbon nucleophiles, and it was noted that all compatible nucleophiles had some combination of nitro, ketone, or ester functionalities. Additionally, eight of the potential nucleophiles were found to be incompatible with the optimal reaction conditions. Mechanistic studies were carried out that supported the hypothesis that this reaction goes through a similar mechanism to that elucidated for the allylic C-H amination reaction. Following this investigation, a computational study was carried out to discover the origins of the complementary regioselectivity profiles reported by Blakey for the allylic C-H amidation of the asymmetric internal olefinic substrate 1-phenylbut-2-ene with *tert*-butyl dioxazolone via Rh(III)Cp* or Ir(III)Cp* catalysis. Using density functional theory calculations with distortion/interaction-activation fragment analysis, it was found that rhodium imbues significantly more distortional strain in the transition state at the rate determining step than iridium does, and this difference leads to complementary regioselectivity profiles. Finally, a study into the invention of a novel chiral indenylrhodium(III) sulfoxide catalyst was undertaken. Previous reports indicated that indenyl ligand scaffolds could catalyze organometallic syntheses with much higher rates, regio-, and enantioselectivity than other popular ligand scaffolds such as cyclopentadienyl ligands. Although the development of a novel chiral indenylrhodium(III) sulfoxide complex is ongoing, its successful synthesis and application in enantioselective allylic C-H functionalization will represent a significant advance in this field by offering unprecedented regio- and stereocontrol of allylic C-H functionalization reactions.

Computational and Experimental Studies of Allylic C-H Functionalization of Internal Olefins via
Group IX Metal- π -Allyl Intermediates and Invention of a Chiral Indenylrhodium(III) Catalyst

By

Thomas Joseph Kowal-Safron

Simon B. Blakey

Adviser

A thesis submitted to the Faculty of Emory College of Arts and Sciences
of Emory University in partial fulfillment
of the requirements of the degree of
Bachelor of Science with Honors

Department of Chemistry

2020

Acknowledgements

I would like to extend my sincerest gratitude to Prof. Simon Blakey for inviting me to be a member of his research group and for having so much faith in me over the past four years. My time as a member of his research group has been a bright spot in my undergraduate career, and I have had a number of incredible experiences that were made possible thanks to his efforts and encouragement of my growth as a chemist.

I would also like to extend a sincere note of thanks to Caitlin Farr, who has been the best graduate student mentor I could have asked for. Working with her has been a tremendous blessing, and I have grown so much as a student, researcher, and person thanks to the many lessons she has taught me both in and out of the lab.

I would also like to thank all the members of the Blakey research group, past and present, who have been there to support me over the past several years. I am particularly grateful for the guidance and encouragement of David Laws, Amaan Kazerouni, Christopher Poff, and Michael Robson Hollerbach on the indenyl-sulfoxide complex project. I am also extraordinarily grateful to Quincy McKoy for providing incredibly helpful feedback on my graduate school application essays that was instrumental in helping me get accepted to my top-choice PhD program.

I would also like to thank all the members of the Baik research group at the Korea Advanced Institute of Science and Technology for being so kind and welcoming during my visit to South Korea in 2019. I would not have been able to perform computational chemistry research without the assistance of Seungha Kim, Mannkyu Hong, and Dasol Cho. I would also like to thank Dr. Jiyong Park, Bohyun Park, and Joonghee Won for working on the project with me. Additionally, this research experience would not have been possible without the tireless efforts of Yunmi Baek and Prof. Mu-Hyun “Mookie” Baik, or the incredibly helpful logistical resources and funding provided by Carolyn Wright and Dr. Dan Morton of the NSF Center for Selective C-H Functionalization’s IRES program.

Finally, I would like to extend a sincere note of thanks to Dr. Antonio Brathwaite, Prof. Cora MacBeth, and Prof. Patricia Marsteller for being on my Honors committee, as well as for the incredible efforts they have made for me over the years that inspired me to ask them to be on this committee. Thank you to Ashley Zachmann for collaborating with me on the allylic C-H alkylation project, to Kim Sharp and Steven Chen for sharing a hood with me in lab over the years, and to all the incredible people I have worked with from the Emory University Department of Chemistry during my time as an undergraduate student.

Table of Contents

1. Introduction	1-6
2. Results and Discussion	6-34
2.1. Allylic C-H Alkylation	6-14
2.2. Probing the Regioselectivity of Rhodium versus Iridium Catalysts	14-28
2.3. Development of a Novel Chiral Indenylrhodium Catalyst	28-34
3. Conclusions and Future Directions	34-36
4. Supplemental Information	36-53
4.1. General Information	36-37
4.2. Materials Preparation	37-51
4.3. Procedures for the Density Functional Theory Calculations	51-53
5. References	53-57

Figures

1. Palladium-catalyzed accession of a π -allyl complex	2
2. Rhodium (III)-catalyzed allylic C-H functionalization of a terminal alkene	2
3. Isolation of a Rh(III) π -allyl complex	3
4. Complementary regioselectivity profiles in allylic C-H amidation	4
5. Illustration of the indenyl “ring slip” phenomenon	5
6. Overview of the reaction conditions subject to optimization for allylic C-H alkylation	7
7. Reaction conditions for the silver mechanistic study	13
8. Reaction conditions for the rhodium mechanistic study	14
9. Complementary regioselectivity profiles in allylic C-H amidation	15
10. General mechanistic hypothesis used to construct energy profiles	19

11. Energy profile of Rh(III)-catalyzed allylic C-H amidation	20
12. Energy profile of Ir(III)-catalyzed allylic C-H amidation	21
13. Molecular orbital diagrams of rhodium intermediates	24
14. Rhodium (III) distortion/interaction-activation fragment analysis	25
15. Iridium (III) distortion/interaction-activation fragment analysis	26
16. Illustrations of the distorted dioxazolone fragments	27
17. Synthetic scheme for the indenyl-sulfoxide ligand scaffold	28
18. Reflux complexation attempts	31
19. Microwave complexation attempt	32
20. Current attempts at complexation	33

Tables

1. Optimization of the dimethyl malonate reaction	8
2. Scope of malonate-type carbon nucleophiles for allylic C-H alkylation	10
3. Transition states for reductive elimination from nitrenoid intermediates	17
4. Transition states for reductive elimination from bidentate intermediates	18

Introduction: Catalytic allylic substitution reactions are highly medicinally relevant reactions that have been the subject of increasing investigation over the past several years. Thanks to many recent innovations, allylic substitution via transition metal π -allyl formation has taken a place on the cutting edge of organotransition metal chemistry.¹⁻⁷ The emerging goal in this field has been to transition from traditional reaction schemes, which generally would require the pre-installation of a leaving group or other functionality, to the accession of transition metal π -allyl complexes via direct C-H functionalization pathways.² The achievement of this goal would enable the innovation of new, diverse synthetic organic methods that would minimize the number of chemical transformations needed and curtail both cost and waste generation.

Pioneering research into the use of transition metal complexes as catalysts in allylic substitution reactions was explored by Tsuji and Trost using palladium complexes. In 1965, Tsuji established that palladium π -allyl complexes are electrophilic and can react with carbon nucleophiles to form new C-C bonds.³ Further research by Trost established useful transition metal catalysts for highly enantioselective allylic alkylation.⁴ In 2008, White and colleagues made the significant advance of developing a palladium catalyst that would use allylic C-H bonds to access π -allyl complexes and eliminate the need for a leaving group in allylic alkylation, as shown below in Figure 1.⁵ This advance made the olefin the limiting reactant and used only mild oxidants, which made the palladium-catalyzed allylic functionalization efficient and viable.

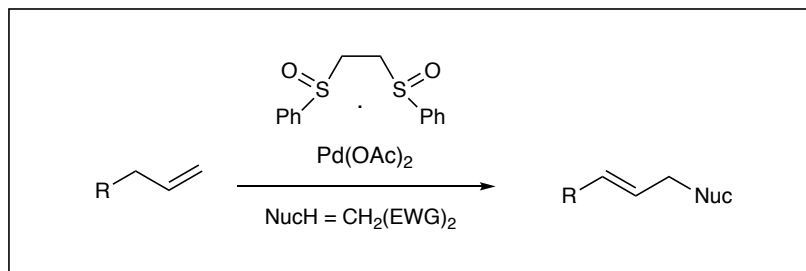


Figure 1. A general schematic of the reactions developed by Christina White in 2008 to access π -allyl complexes via allylic C-H bonds using a palladium catalyst.

Although palladium complexes were used in much of the pioneering research, they had several critical limitations. Perhaps the most significant of these was that the carbon nucleophiles used had to be stabilized (e.g. malonate). This limited the scope of viable carbon nucleophiles that could be used in these types of reactions.³⁻⁵ Additionally, in all reported cases of palladium-catalyzed C-H functionalization reactions, only monosubstituted olefins were suitable substrates.³⁻⁵

In light of the limitations presented by palladium complexes, a transition was made to Group IX metal complexes, with a particular interest in rhodium (III) and iridium (III). In 2012, Cossy was the first to access allylic C-H functionalization of an internal alkene via a Rh(III) catalyst, as depicted below in Figure 2.⁶

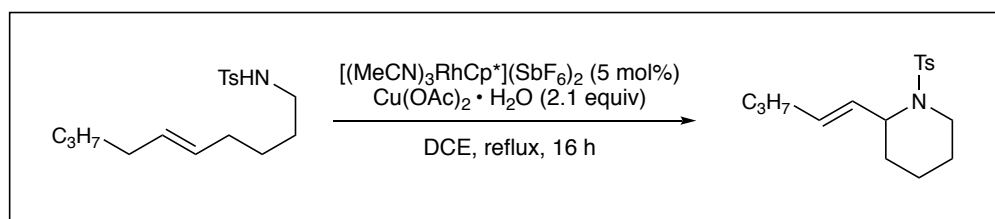


Figure 2. The first reported example of the allylic C-H functionalization of an internal alkene via a Rh(III) catalyst. This reaction was developed by Cossy in 2012.

At the time this reaction was developed, the standing hypothesis was that Group IX metal complexes can catalyze C-H functionalization via π -allyl intermediates to form new C-C bonds.

In 2016, Tanaka and coworkers isolated a π -allyl intermediate from a C-H functionalization reaction that was formed from a cyclopentadienylrhodium complex, $[\text{RhCp}^{\text{E}}\text{Cl}_2]_2$, which is shown below in Figure 3. In that study, π -allyl intermediates from both mono- and disubstituted olefin substrates were isolated.⁷

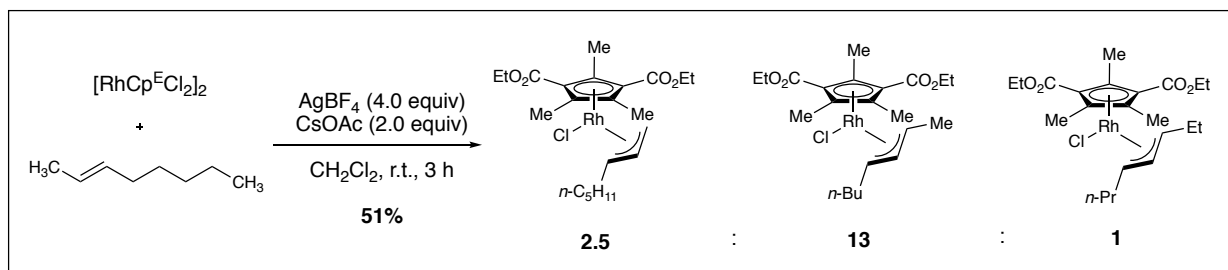


Figure 3. The reaction used by Tanaka in 2016 to generate an isolatable Rh(III) π -allyl complex.

Since this development by Tanaka, much seminal work has been done to harness the utility of π -allyl intermediates in Group IX metal-catalyzed C-H functionalization reactions.⁸⁻¹⁰ Investigations by Blakey and colleagues have led to the establishment of a wide scope of compatible nucleophiles for the formation of novel C-N and C-O bonds, but the invention of reactions to form new C-C bonds via direct C-H functionalization has been met with a few unique challenges.^{8,9} This is mainly because carbon nucleophiles have been traditionally more difficult to work with due to the issues described previously. As a result, recent attention has been focused on developing reactions to form C-C bonds via direct C-H functionalization. One such example of these investigations, the development of Rh(III)-catalyzed allylic C-H alkylation reactions of disubstituted olefins with malonate-derivative nucleophiles, is described herein.

Following the elucidation of the wide scope of compatible nucleophiles for the formation of C-N, C-O, and C-C bonds with symmetric disubstituted olefin substrates via direct C-H functionalization, attention was turned to the resulting regio- and stereoselectivities imbued by

this reaction pathway on asymmetric disubstituted olefins.¹⁰ In a 2019 study, Blakey reported an intriguing set of complementary regioselectivity profiles in allylic C-H amidation reactions that were dependent on the metal used in the catalytic complex – rhodium versus iridium.¹⁰ The differential regioselectivity profiles are summarized below in Figure 4.

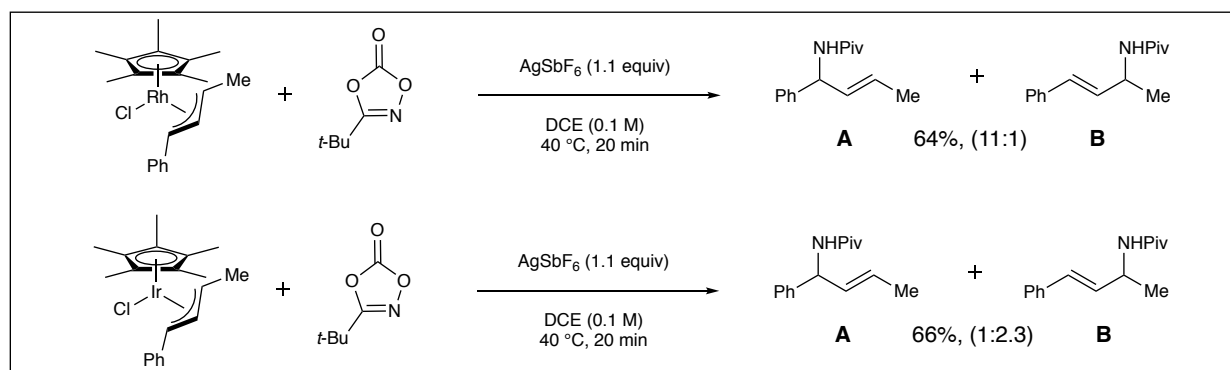


Figure 4. The complementary regioselectivity profiles from allylic C-H amidation reactions reported by Blakey in 2019.

This result was unexpected based on both the isoelectronic nature of the rhodium (III) and iridium (III) metal centers as well as the identical ligand scaffolds on each metal center. In light of this result, as well as a 2016 study by Chang and Baik that explored a notable difference in reaction rates between similarly identical rhodium and iridium complexes, increased interest was given to the elucidation of the origins of observed differences in regio- and stereoselectivity in allylic C-H functionalization reactions that appeared to arise solely on the basis of the metal used in the catalytic complex.¹¹ A computational study that constructed complete energy profiles to compare the rhodium- versus iridium-catalyzed C-H amidation reactions shown above in Figure 4 and elucidate what is responsible for the differential regioselectivity profiles is reported herein.

Since the inception of this area of research into transition metal-catalyzed allylic C-H functionalization, much focus has been directed toward transition metal complexes with

cyclopentadienyl ligands.⁸⁻¹⁰ However, in the field of organometallic catalysis in general, another emerging trend has been to invent chiral indenylmetal catalysts.¹²⁻¹⁵ Interest in this area has been generated due to the impacts of reactivity in catalytic synthetic processes caused by the unique properties of indenyl ligands.¹² Interest in aromatic ligand scaffolds was sparked by the 1952 elucidation of the bonding structure of ferrocene by Wilkinson, Woodward, and Fischer, which established the cyclopentadienyl (Cp) ligand as a cornerstone in organometallic catalysis.¹² Further research by Hart-Davis and Mawby demonstrated that the fusion of an additional benzo ring to the Cp ring to form an indenylmetal complex resulted in a significant acceleration of catalytic organometallic reactions.¹²

The acceleration of reaction rates in the presence of indenylmetal catalysts has been attributed to the ease with which the indenyl ligand can “slip” between the η^5 and η^3 coordination modes.¹³ This η^5 to η^3 “ring slip” opens an additional coordination site without changing the oxidation state of the metal, which accelerates the rate of organometallic catalysis by facilitating the coordination step of the catalytic cycle.¹³ A detailed depiction of the “ring slip” phenomenon is shown below in Figure 5.

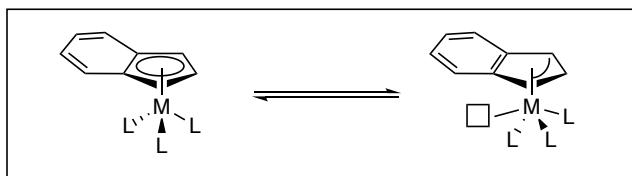


Figure 5. An illustration of the “ring slip” phenomenon in which the indenyl ligand changes between the η^5 and η^3 coordination mode, opening an additional coordination site without changing the oxidation state of the metal center.

In addition to their application in the acceleration of organometallic catalysis, indenyl ligands are also of interest due to their different steric profile than cyclopentadienyl ligands.¹³ This different steric profile is potentially useful for asymmetric catalysis.¹³ Previous

enantioselective syntheses via asymmetric catalysis with chiral indenylmetal complexes have utilized indenylzirconium and indenylcobalt complexes.^{14, 15}

Preliminary investigations by the Blakey research group utilizing an indenylrhodium complex, rather than an established cyclopentadienylrhodium catalyst, have demonstrated their potential to catalyze allylic C-H functionalization reactions with remarkable enantioselectivity.¹⁶ However, a significant obstacle to the increase in the prevalence of indenylmetal complexes in catalysis is the lack of reliability with which they can be stereospecifically synthesized.¹⁷ In light of this difficulty, attention among organometallic chemists has been turned toward investigating methods for facially selective π -complexation.¹⁷ A 2012 study by Baker resulted in the first reported example of enantio- and diastereospecific syntheses of planar chiral bidentate Cp-sulfanyl and -sulfinyl complexes thanks to the incorporation of axially chiral indenyl ligands.¹⁷ Inspired by both this study and the previously discussed preliminary investigations of the Blakey group, another investigation into the synthesis of a chiral bidentate indenyl-sulfoxide rhodium (III) complex has been undertaken and is reported herein. Further studies on the reactivity and catalytic aptitude of this complex are ongoing.

Results and Discussion:

Allylic C-H Alkylation

To undertake the study of allylic C-H alkylation with malonate-derivative carbon nucleophiles, 1,3-*trans*-diphenylpropene was chosen as a model substrate. This was because this olefin is a small, symmetric, internal olefin, which would simplify product analysis by eliminating the potential problem of differential regio- and stereochemistry unless a given nucleophile came with a pre-installed asymmetric carbon center. To begin the study, a series of

reaction condition optimization experiments were conducted using dimethyl malonate as the model nucleophile with $[\text{RhCp}^*\text{Cl}_2]_2$ as the catalyst, AgSbF_6 as a halide scavenger to activate the catalyst, AgOAc as an oxidant, and 1,2-dichloroethane as the solvent. The reaction conditions are illustrated below in Figure 6. The productivity of these reactions was monitored by ^1H NMR using 1,4-dinitrobenzene as an internal standard to measure yield.

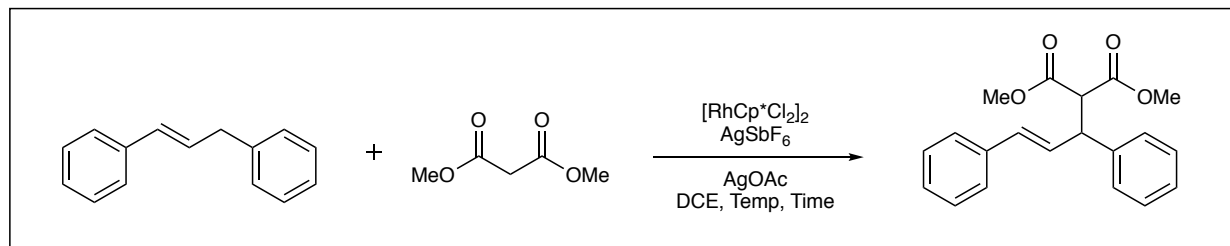


Figure 6. A general schematic of the necessary reagents and reaction conditions subject to optimization in this study.

Previous studies conducted in the Blakey group to investigate allylic C-H amination and etherification had established 2.1 equivalents of AgOAc as the optimal amount. However, each of the other factors were potentially variable depending on the type of bond (e.g. C-O, C-N, or C-C) that was being formed. As such, it was necessary to optimize the reaction conditions shown above in Figure 6. The results of this optimization study are shown below in Table 1 and are described here in detail. The initial experiments were to vary the time and temperature of the reactions. As shown in Table 1, the initial reactions at 40 °C for both 6 and 24 hours did not yield any product. As a result, the temperature was subsequently raised, as reactions that take more than 24 hours, unless absolutely necessary, are generally regarded as insufficiently efficient for implementation in larger scale, pharmaceutically relevant syntheses.

Table 1. Results of the optimization study for the reaction of dimethyl malonate with 1,3-*trans*-diphenylpropene.

Entry	Temp (°C)	Time (h)	[Rh] (mol%)	Nuc. (equiv)	% Yield ^a
1	40	6	2.0	2.5	n.d.
2	40	24	2.0	2.5	n.d.
3	60	6	2.0	2.5	n.d.
4	60	24	2.0	2.5	73
5	80	6	2.0	2.5	62
6	80	24	2.0	2.5	78
7	80	24	1.0	2.5	44
8	80	24	2.5	2.5	75
9	80	24	5.0	2.5	n.d.
10	80	24	2.5	1.25	76
11	80	24	2.5	5.0	99

[a] Yields were determined by ¹H NMR using 1,4-dinitrobenzene as an internal standard.

As shown in Table 1, the increased temperature enabled the reaction to proceed more efficiently. At 60 °C, although no product was observed at the 6-hour time point, a yield of 73% was measured according to the internal standard after 24 hours. Because of the increased yield that came from increasing the temperature, another 20 °C temperature increase was done, and the reaction was then carried out at 80 °C. As shown in Table 1, the yield was 62% as measured by the internal standard after 6 hours, and 78% after 24 hours.

After establishing reaction conditions that enabled the sufficiently fast generation of the product, the next step was to investigate how altering the amounts of the different reagents would impact the overall yield of the reaction. In the interest of more sustainable reaction development,

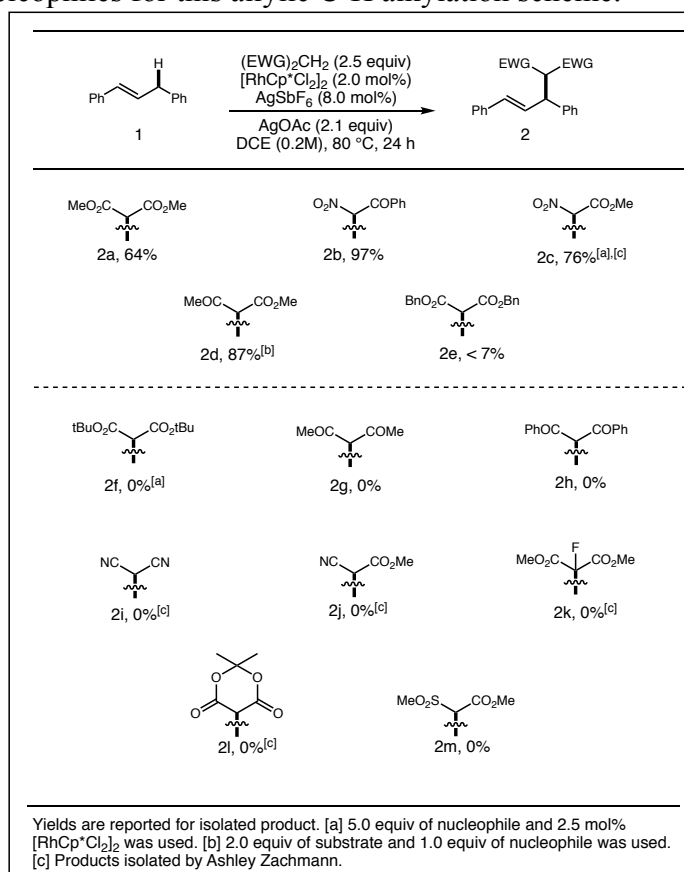
the first new set of conditions involved halving the catalyst loading from 2.0 mol% to 1.0 mol%. As shown in Table 1, this was detrimental to the yield, lowering it to 44%. Next, the catalyst loading was raised by 20% from the initial set of reaction conditions, from 2.0 mol% to 2.5 mol%, which resulted in approximately the same yield as those initial conditions (78% in the initial conditions versus 75% in this experiment). Since this difference was not significant, the catalyst loading was subsequently doubled to determine if more catalyst translated to higher yield. Interestingly, it was observed that doubling the catalyst loading to 5.0 mol% shut down the reaction and resulted in no discernible product formation, along with the partial degradation of the starting material into unidentified products in the crude reaction mixture. It is plausible that the higher catalyst loading allowed for the simultaneous generation of a larger number of reactive intermediates that subsequently reacted with each other in an off-pathway fashion that curtailed product formation.

Finally, the impact of changing the amount of nucleophile present in the reaction mixture was investigated. First, the amount of nucleophile was halved from 2.5 equivalents relative to the olefin to 1.25 equivalents. As shown in Table 1, this resulted in an insignificant, slight reduction of the yield from 78% to 76%, as measured by the internal standard. The amount of nucleophile was then doubled from the initial reaction conditions to 5.0 equivalents, which resulted in a 99% yield as measured by the internal standard. With seemingly optimal reaction conditions in hand, the focus was then shifted to isolating the product and screening a scope of malonate-derivative carbon nucleophiles for compatibility with these reaction conditions.

Initial attempts at isolation of the dimethyl malonate product via the standard method of flash column chromatography proved futile due to the intense difficulty that arose in separating the desired product from excess nucleophile left over in the crude reaction mixture. After several

failed attempts and much time spent developing column conditions to achieve optimal separation, it was concluded that 5.0 equivalents of the nucleophile left far too much unreacted nucleophile in the crude reaction mixture for effective separation. Thus, although the yield according to the internal standard in the ^1H NMR was approximately quantitative, almost half of the product was lost in the isolation scheme because it could not be effectively separated from leftover unreacted nucleophile. Therefore, it was decided for the sake of facile isolation of the product via flash column chromatography, that it would be best to revert to the initial set of “optimal” reaction conditions that produced a 78% yield at 80 °C over 24 hours according to the internal standard. After making this change, the dimethyl malonate product was isolated at a 64% yield, as shown below in Table 2.

Table 2. Results from the investigation into the scope of potentially compatible malonate-derivative carbon nucleophiles for this allylic C-H alkylation scheme.



Following the successful synthesis and isolation of the dimethyl malonate product, a scope of other malonate-derivative carbon nucleophiles was investigated for compatibility with these reaction conditions. These experiments were done in collaboration with another former member of the Blakey group, Ashley Zachmann. The collective results of this reaction scope, shown above in Table 2, demonstrated that malonate-type carbon nucleophiles with ester, ketone, and nitro functionalities were generally the most readily compatible with the reaction conditions developed in this investigation. It is thought that these functional groups enable sufficient resonance stabilization following the deprotonation of the central carbon of the malonate to generate the active carbon nucleophile in a facile manner. The trend in yield, which was that the nitro-ketone (product 2b) resulted in a higher yield than the nitro-ester (product 2c), which consequently resulted in a higher yield than the di-ester (product 2a), can be explained by differences in the polarity of these substituents. In other words, the large dipole created by combining the nitro group with the ketone results in highly favorable deprotonation of the central carbon, and the magnitude of this dipole diminishes in the inverse order of the trend described above. Thus, the functional groups attached to the malonate-derivative nucleophiles are important for the facilitation of the reaction and are directly correlated with the observed yields.

Also notable from Table 2 are the observed yields of the keto-ester and di-benzyl-ester products. As shown in the table, the keto-ester nucleophile resulted in a relatively high yield of 87% (product 2d), whereas the di-benzyl-ester nucleophile generated a yield of less than 7% (product 2e). These observations are again explained by the relative polarity of the substituents on the carbon nucleophiles. The keto-ester is conducive to deprotonation of the central carbon to generate the active nucleophile and facilitate the reaction, whereas the di-benzyl-ester is much less so due to the stability generated by the aromatic rings on the benzyl substituents.

While there were many promising results from the malonate-derivative carbon nucleophile scope that seemingly indicated broad applicability of these reaction conditions, there were also many nucleophiles that were not tolerated in this system. In light of the successes observed with the dimethyl malonate and both the keto-ester and nitro-ketone, it was somewhat surprising to see that neither di-*tert*-butyl malonate (product 2f in Table 2) nor the di-ketones (products 2g and 2h) were viable nucleophiles. In all three of these cases, it is thought that off-pathway reactions are degrading the nucleophiles before they enter the catalytic cycle. Also notable was the fact that both nucleophiles with nitrile functional groups were incompatible with these reaction conditions (products 2i and 2j). This is likely because of the affinity of nitrile ligands for rhodium, as coordination by the wrong atom (e.g. the nitrogen of the nitrile group of these proposed nucleophiles) would bind up the rhodium, deactivating it and prematurely stopping the reaction.

Given the success of the malonate-derivative nucleophiles with electron-withdrawing functional groups around the central carbon in these reaction conditions, dimethyl malonate with a fluorine substituted at the central carbon was investigated for compatibility in the reaction. However, as shown by the entry for product 2k in Table 2, the fluorine apparently inhibited the reactivity of the malonate and the reaction did not proceed as hypothesized to any detectable desired product. The final two nucleophiles tested were the cyclic di-ester and the sulfonyl ester, shown in the entries for products 2l and 2m in Table 2. As shown in the table, neither of these malonate derivatives were compatible with the reaction conditions developed in this system. The cyclic di-ester was likely incompatible due to its high potential for decomposition under acidic conditions. The mechanism for allylic C-H amination elucidated by the Blakey group generates acetic acid as a side product, thus creating an acidic reaction mixture over the course of the

reaction.² Thus, if this reaction follows a similar mechanism, it is likely that acetic acid is accumulating and degrading the cyclic di-ester before it is deprotonated to react in the desired pathway. Finally, it is likely that the sulfonyl ester was incompatible with these reaction conditions due to off-pathway reactions that would be exacerbated by the presence of the sulfone functional group.

Following the completion of the investigation of the scope of potential malonate-derivative carbon nucleophiles, two brief mechanistic studies were undertaken in order to investigate whether this allylic C-H alkylation reaction pathway follows a similar mechanism to that which was elucidated for allylic C-H amination. In the mechanism for allylic C-H amination, following the redox catalytic cycle, diphenylallyl acetate is produced via reductive elimination, and this species then reacts with a Lewis acid present in the reaction mixture to generate the desired product via an S_N1 mechanism.⁸ For this mechanistic pathway to be plausible in this case of allylic C-H alkylation, some reactant(s) present in the mixture must be able to act as a Lewis acid to generate the products from diphenylallyl acetate. It has been hypothesized that the two most likely candidates to assume this role are AgSbF₆, which is necessary as a halide scavenger to activate the catalytic pathway, and the Rh(III) center of the active catalyst. As a result, the first mechanistic study was a reaction of diphenylallyl acetate with dimethyl malonate and AgSbF₆, shown below in Figure 7. This reaction generated the dimethyl malonate-substituted allylic product in 43% yield.

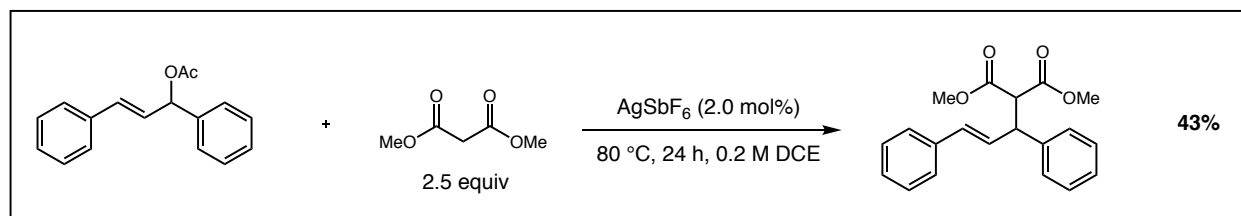


Figure 7. The reaction conditions used for the first mechanistic study in which AgSbF₆ was probed as a Lewis acid.

The second mechanistic study was a similar reaction of diphenylallyl acetate and dimethyl malonate, but this time in the presence of $[\text{RhCp}^*(\text{MeCN})_3](\text{SbF}_6)_2$, which is a monomeric Rh(III) complex. This reaction is shown below in Figure 8, and generated the dimethyl malonate-substituted product in 66% yield. Since both of these species proved to promote the conversion of diphenylallyl acetate to the desired product, and are present in the optimized reaction conditions of 1,3-*trans*-diphenylpropene with dimethyl malonate, there is some support that the diphenylallyl acetate intermediate could be formed in the actual mechanism, and then react with the malonate-type carbon species in a Lewis-acid-catalyzed $\text{S}_{\text{N}}1$ fashion to generate the desired product. Progression through this mechanistic pathway would be consistent with the frequently observed degradation or off-pathway reactivity of many of the malonate-derivative carbon species, as the amount of time needed to generate the diphenylallyl acetate species is more than sufficient for fast, off-pathway degradation reactions to occur.

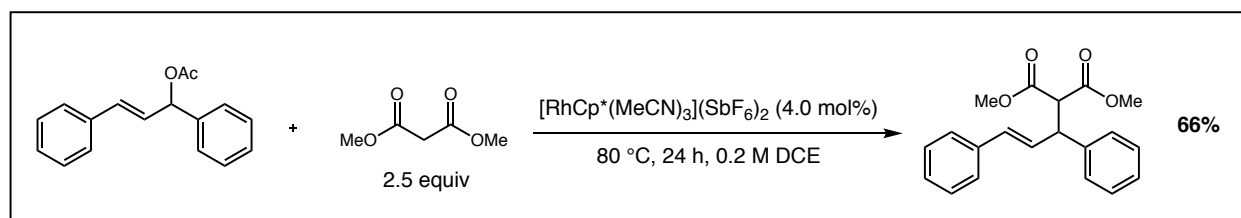


Figure 8. The reaction conditions used for the second mechanistic study, done by Ashley Zachmann, in which $[\text{RhCp}^*(\text{MeCN})_3](\text{SbF}_6)_2$ was probed as a Lewis acid.

Probing the Regioselectivity of Rhodium versus Iridium Catalysts

A 2019 report by Blakey and coworkers revealed a marked regioselectivity difference in the allylic C-H amidation of the asymmetric internal olefinic substrate 1-phenylbut-2-ene with *tert*-butyl dioxazolone when a Rh(III)Cp* catalyst was used versus when an Ir(III)Cp* catalyst was used. The difference is summarized below in Figure 9, which is a replication of Figure 4. At the time this observation was published as part of a larger study on allylic C-H amidation, the

reasons for the observed difference in regioselectivity and the mechanism of the reaction were subject to educated conjecture. To determine the energetic underpinnings of the regioselectivity difference and develop a plausible mechanistic proposal, a computational study was undertaken to develop complete reaction energy diagrams for both the Rh(III)- and Ir(III)-catalyzed allylic C-H amidation reactions.

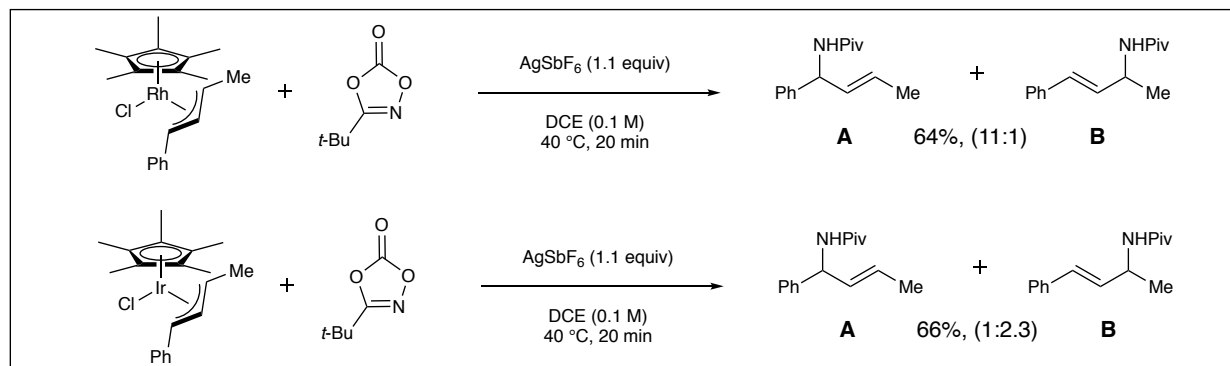


Figure 9. The complementary regioselectivity profiles from the allylic C-H amidation reactions reported by Blakey in 2019.

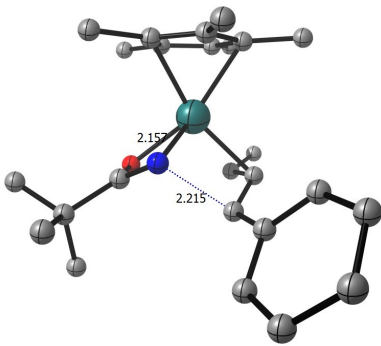
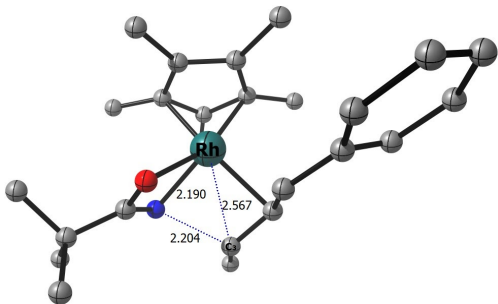
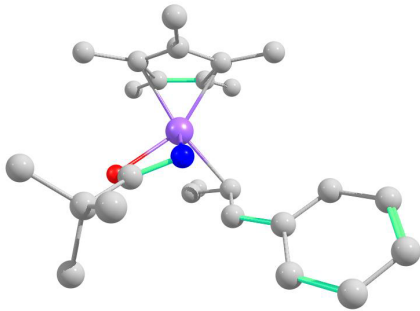
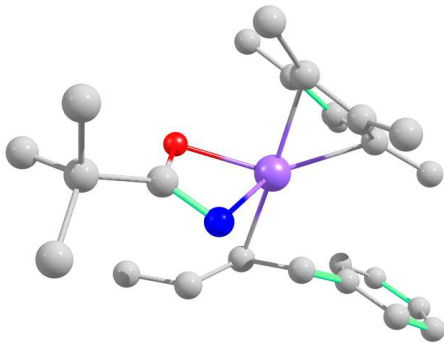
The first hypothesis raised in this study was that the regioselectivity difference could be attributable to a difference in the manner in which the *tert*-butyl dioxazolone coordinates to the catalytic metal center. Based on the reactions depicted above, to transform from the dioxazolone reagent to the observed product, one equivalent of carbon dioxide would need to be eliminated at some point during the reaction. Thus, one could envision two possible coordination modes. First, the dioxazolone could coordinate to the metal center in a monodentate fashion with the lone pair of electrons on the nitrogen before subsequently releasing the carbon dioxide and remaining bound to the metal center in a nitrenoid fashion. Alternatively, the dioxazolone could release the carbon dioxide before coordinating, and then coordinate in a bidentate fashion via both the lone pair on the nitrogen and a lone pair from the resulting anionic oxygen.

Density functional theory (DFT) calculations were used to determine which of these coordination modes was most plausible. However, to begin the DFT calculations, two assumptions needed to be made about the nature of the reaction mechanism. First, it was assumed that the silver present in the reaction mixture acted solely as a halide abstractor and did not oxidize the metal center. Secondly, it was assumed that the last step of the mechanism involved a reductive elimination reaction to form the product. With these assumptions in hand, the first set of DFT calculations was undertaken to locate the transition states for the reductive elimination from each of the mono- and bidentate intermediates to the products of addition at both the C₁- and C₃-positions. The results of these calculations, for both Rh(III) and Ir(III) metal centers, are shown below in Tables 3 and 4.

Table 3. A summary of the findings for the transition states of the proposed reductive elimination step to form the C₁- and C₃-amidated products from a monodentate intermediate in which the dioxazolone is coordinated to the metal center in a nitrenoid fashion via the nitrogen atom only. The $\Delta\Delta G^\ddagger$ values indicated in the table are the differences in energy between the transition states shown and the lowest-energy transition states for both mono- and bidentate intermediates (i.e. considering both the data in this table and Table 4) for each different metal center (e.g. rhodium or iridium). The data for the rhodium transition states was computed by Dr. Jiyong Park.

	C₁ Transition State	C₃ Transition State
Rhodium		
$\Delta\Delta G^\ddagger$	3.56 kcal/mol	1.86 kcal/mol
Iridium		
$\Delta\Delta G^\ddagger$	1.25 kcal/mol	0.00 kcal/mol

Table 4. A summary of the findings for the transition states of the proposed reductive elimination step to form the C₁- and C₃-amidated products from a bidentate intermediate in which the dioxazolone is coordinated to the metal center via lone pairs on both the oxygen and nitrogen atoms. The $\Delta\Delta G^\ddagger$ values indicated in the table are the differences in energy between the transition states shown and the lowest-energy transition states for both mono- and bidentate intermediates (i.e. considering both the data in this table and Table 3) for each different metal center (e.g. rhodium or iridium). The data for the rhodium transition states was computed by Dr. Jiyong Park.

	C₁ Transition State	C₃ Transition State
Rhodium		
$\Delta\Delta G^\ddagger$	1.46 kcal/mol	0.00 kcal/mol
Iridium		
$\Delta\Delta G^\ddagger$	4.86 kcal/mol	12.82 kcal/mol

Interestingly, it was noted that for the Ir(III) metal center, the monodentate coordination mode was much lower in energy, whereas the opposite was the case for the Rh(III) metal center. Thus, it was initially thought that this blatant difference was responsible for the observed

differences in regioselectivity. However, as further DFT calculations were carried out to develop complete energy profiles for these reactions, it was discovered that the formation of a 4-membered rhodocycle intermediate was not energetically permissible.¹⁸ Thus, for the remainder of the calculations, it was assumed that the proper coordination mode was the monodentate mode. As a result, the mechanistic hypothesis depicted below in Figure 10 was used to calculate the complete energy profiles for both the Rh(III)- and Ir(III)-catalyzed reactions.

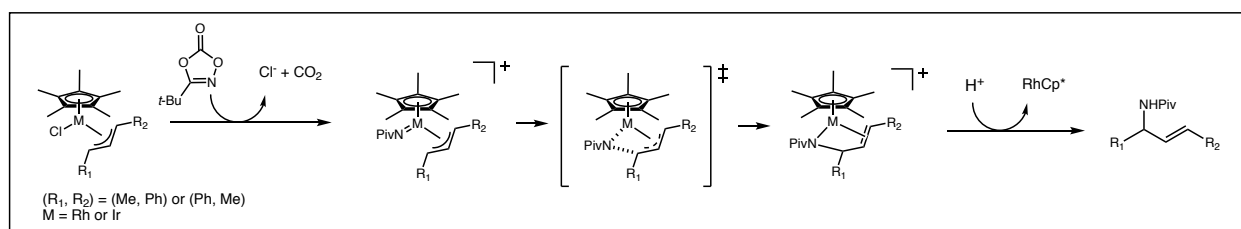


Figure 10. The general mechanistic hypothesis used to construct the energy profiles for the rhodium- and iridium-catalyzed allylic C-H amidation reactions. Note that the reactions begin with a Metal (III) center and proceed through a transient Metal (V) nitrenoid intermediate.

With the preliminary results and assumptions described before, the complete energy profile for the Rh(III)-catalyzed reaction was computed by Dr. Jiyong Park, with whom this computational study was undertaken as a collaborative effort. The resulting energy diagram is shown below in Figure 11.

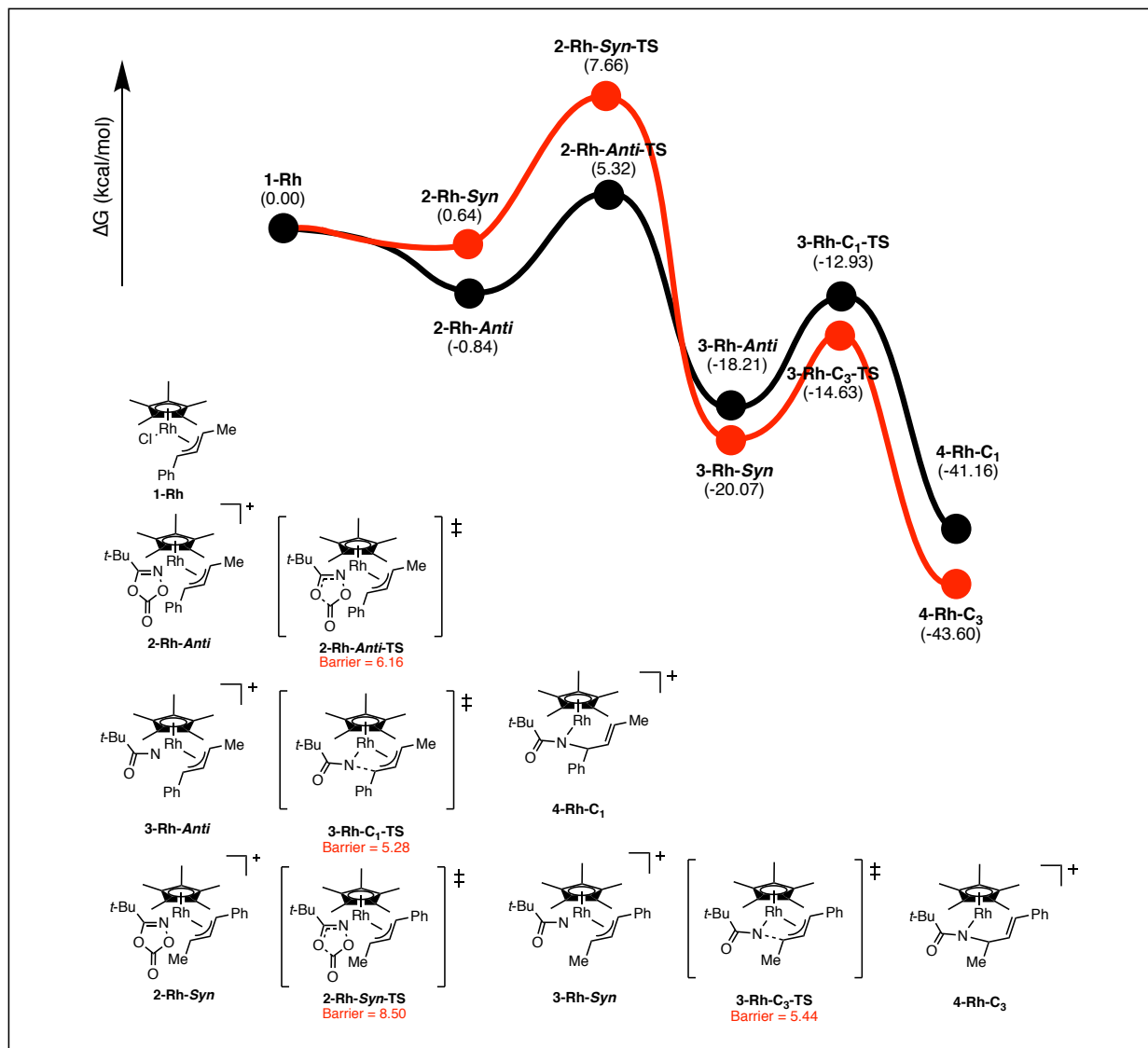


Figure 11. The complete energy profile of the Rh(III)-catalyzed allylic C-H amidation reaction. In the structures depicted with the labels from the energy diagram, “Syn” and “Anti” refer to the relative positions of the *tert*-butyl group of the dioxazolone and the phenyl group of the allylic substrate. All numerical values represent units of kcal/mol. The numbers in parentheses are relative to the energy of Structure **1** while the “Barriers” highlighted in red text are relative to the previous stable intermediate (e.g. **3-Rh-C₁-TS** is 5.28 kcal/mol higher in energy than **3-Rh-Anti**). The data for this figure was produced by Dr. Jiyong Park.

At the same time, the completed energy profile for the Ir(III)-catalyzed reaction was calculated and is shown below in Figure 12.

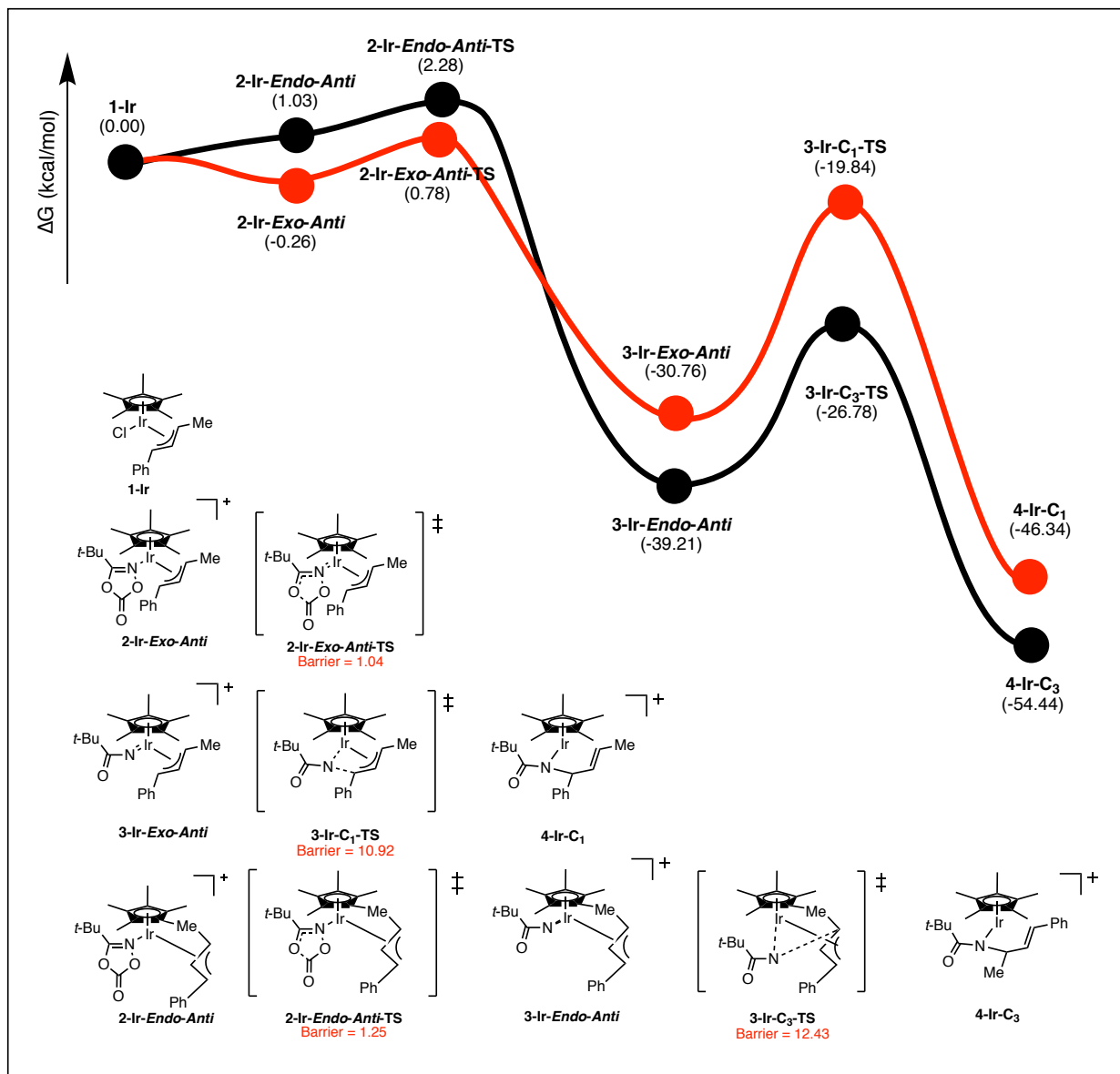


Figure 12. The complete energy profile of the Ir(III)-catalyzed allylic C-H amidation reaction. In the structures depicted with the labels from the energy diagram, “*Syn*” and “*Anti*” refer to the relative positions of the *tert*-butyl group of the dioxazolone and the phenyl group of the allylic substrate. Additionally, “*Endo*” and “*Exo*” refer to the relative positions of the central carbon of the allylic portion of the allylic substrate (i.e. C₂) and the iridium metal center. All numerical values represent units of kcal/mol. The numbers in parentheses are relative to the energy of Structure 1 while the “Barriers” highlighted in red text are relative to the previous stable intermediate (e.g. **3-Ir-C₁-TS** is 10.92 kcal/mol higher in energy than **3-Ir-Exo-Anti**).

The energy profiles calculated for the Rh(III)- and Ir(III)-catalyzed reactions elucidated a plausible explanation of the observed difference in regioselectivity. According to the rhodium energy profile, the carbon dioxide removal step has an energy barrier of 6.16 or 8.50 kcal/mol,

depending on the conformation of the coordinated dioxazolone. Since the barrier for reductive elimination is 5.28 or 5.44 kcal/mol, it can be concluded that the carbon dioxide removal is the rate determining step in this mechanistic pathway.

Alternatively, in the case of the iridium reaction, the barrier to carbon dioxide removal is just 1.04 or 1.25 kcal/mol. The reductive elimination step, however, has a barrier of 10.92 or 12.43 kcal/mol. Thus, it can be concluded that for the iridium reaction, the reductive elimination is the rate determining step. This difference in rate determining step is important to the explanation of the difference in regioselectivity. In the case of the Ir(III)-catalyzed reaction, because the difference in the barrier to carbon dioxide removal (depending on the conformation of the coordinated dioxazolone) is much lower than in the Rh(III)-catalyzed reaction, the iridium is relatively indiscriminate about the conformation of the dioxazolone. Therefore, although the conformation that leads to the C₁-addition product is preferred, the one leading to C₃-addition is relatively well-tolerated. This allows the reaction to equilibrate to the thermodynamically favorable nitrenoid intermediate, which is the one that leads to the C₃-addition product.

However, in the case of the Rh(III)-catalyzed reaction, the difference in the barrier to carbon dioxide removal depending on the conformation of the coordinated dioxazolone is much higher. As a result, one conformation is clearly preferable to the other prior to the carbon dioxide removal step. So, the dioxazolone has more time to detach from an energetically unfavorable conformation and reattach in the more energetically favorable conformation. Because the energetically favorable conformation is the one that leads to C₁-addition, the carbon dioxide removal step dictates that the regioselectivity of the rhodium reaction is complementary to that of the iridium reaction. This is the key explanation for the observed difference in regioselectivity between rhodium and iridium.

This rationale is further supported by DFT calculations of the molecular orbitals of the nitrenoid intermediates for the Rh(III)-catalyzed reaction, the results of which are shown below in Figure 13. These calculations, done by Dr. Jiyong Park, demonstrated that there is extensive π -conjugation from the rhodium center to the oxygen of the pivalate. Thus, the calculations support the fact that each bond in this conjugated system has an order such that rotation about the bond is improbable at the experimental temperature. As a result, it can be concluded that once the nitrenoid intermediate is formed, its conformation is locked and the reaction will result in the products indicated in the energy profiles at the end of the reaction. In other words, the formation of the nitrenoid intermediate is a “committing” step, meaning that the eventual product of the entire reaction is determined based on the conformation of the nitrenoid intermediate. Therefore, the conformation of the coordinated dioxazolone is crucial in the determination of which regioisomer is formed in each reaction, as this directly impacts the conformation of the nitrenoid intermediate formed upon the removal of carbon dioxide.

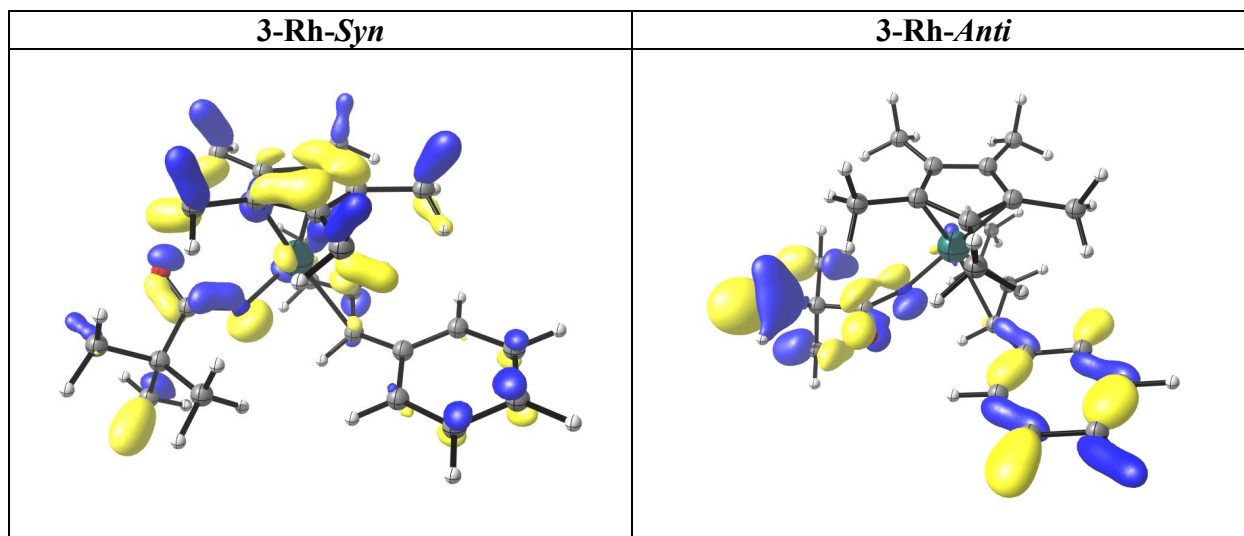


Figure 13. Results from the molecular orbital DFT calculations of the **3-Rh-Syn** and **3-Rh-Anti** reactive intermediates that show the extensive π -conjugation from the rhodium metal center through the oxygen of the pivalate in both intermediates. This π -conjugation gives all the involved bonds partial-double-bond character, which restricts their ability to rotate. The implication of this in reactivity is that these two intermediates are not kinetically interchangeable after the carbon dioxide removal step of the reaction mechanism. Although calculations for the respective iridium intermediates were not done, it is thought that the same principle applies based on these results and the isoelectronic nature of the rhodium and iridium centers used in these reactions. The data used for this figure was produced by Dr. Jiyong Park.

To attempt to explain the energetic reasons for the differential stability of the various conformations of the coordinated dioxazolone that evidently depended on the metal center, an investigation of the carbon dioxide removal step was undertaken using a computational technique known as distortion/interaction-activation fragment analysis.¹⁹ Essentially, the transition states for the carbon dioxide removal step were split into two fragments: the metal complex fragment and the dioxazolone fragment. After splitting the total complex into these two fragments, the strain energies were calculated to determine which parts of the complex at the transition state were most strained and thus contributing the most to the energy barrier to the reaction. The results of these calculations, which gave both the energy of the distortion strain and the stabilization caused by the electronic interactions between the fragments to give the net change in free energy, are summarized below in Figures 14 and 15.

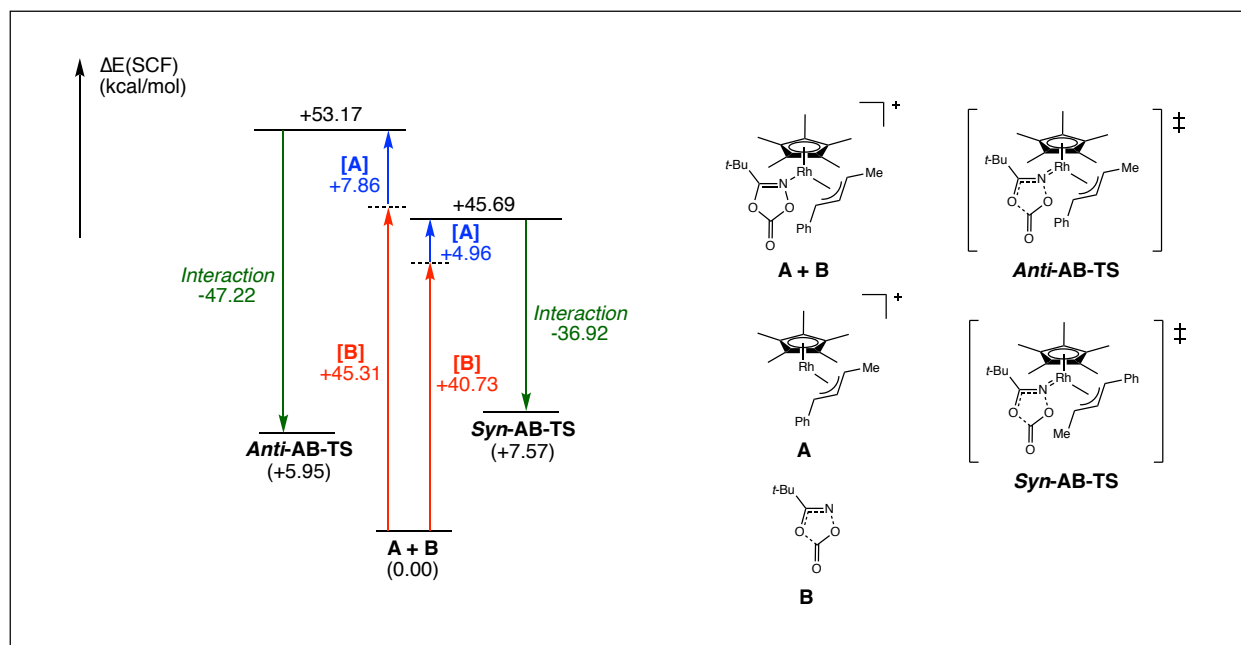


Figure 14. A summary of the results of the distortion/interaction-activation fragment analysis for the carbon dioxide removal step in the Rh(III)-catalyzed allylic C-H amidation reaction. As is shown in the figure, the dioxazolone fragments account for significantly more of the distortional strain energy than the metal center fragments do in the transition state of this step in the reaction pathway. Results for both the *Anti* and *Syn* transition states are shown.

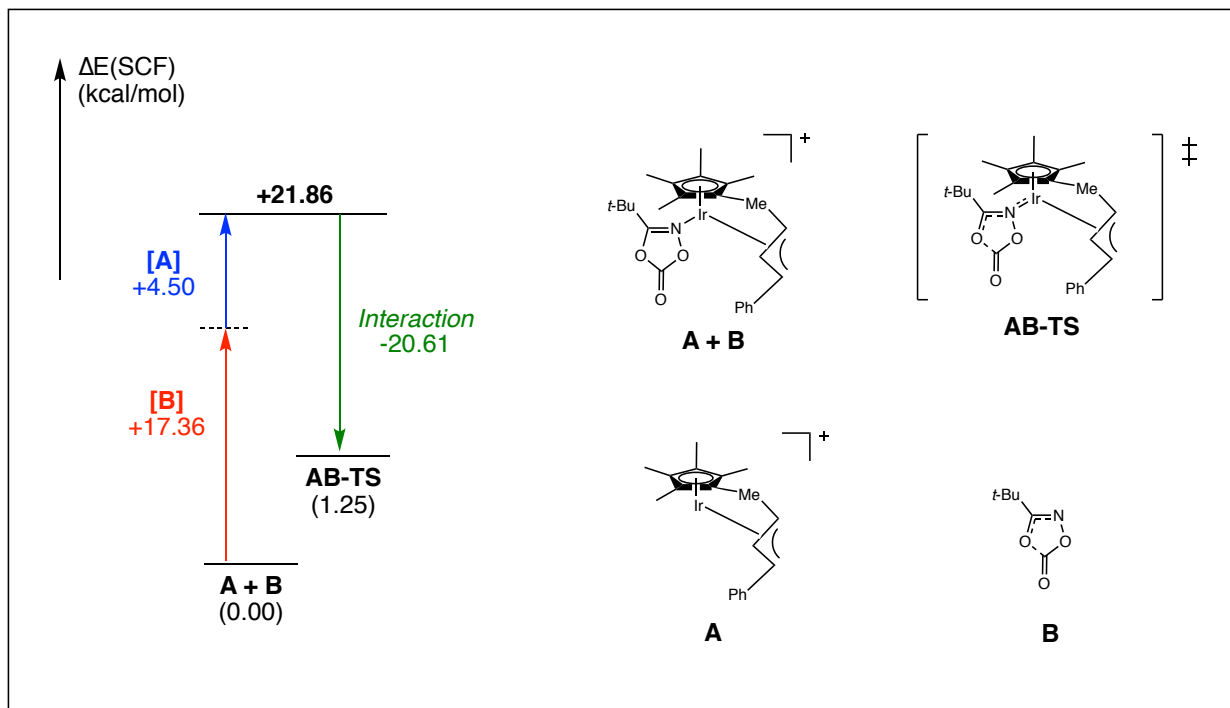


Figure 15. A summary of the results of the distortion/interaction-activation fragment analysis for the carbon dioxide removal step in the Ir(III)-catalyzed allylic C-H amidation reaction. As is shown in the figure, the dioxazolone fragment accounts for significantly more of the distortional strain energy than the metal center fragment does in the transition state of this step in the reaction pathway. Results for only the *Endo* transition state are shown because the calculations for the *Exo* transition state failed. However, due to the significant difference in the dioxazolone strain shown here versus that shown in Figure 14 (compare the arrows for the [B] fragments in both figures), it was decided that a reasonable comparison could be made based on the data presented in these two figures.

The most important result from the fragment analysis calculations was that the dioxazolone fragment of the rhodium complex was significantly (almost 3-fold) more strained than its counterpart in the iridium complex. As shown in Figures 14 and 15, the strains on the metal complex fragments were fairly similar. Therefore, the likely reason that these metals react differently in this allylic C-H amidation pathway is that they cause different amounts of strain on the dioxazolone fragments during their interactions in the transition state of the carbon dioxide removal step. This differential strain on the reacting dioxazolone causes different coordinating conformations to be favored depending on whether the metal center is rhodium or iridium,

which, as described previously, eventually leads to different regioisomeric products in this allylic C-H amidation pathway. Thus, this analysis strongly indicates that the underlying reason for the observed difference in regioselectivity is that the different metal centers imbue significantly different amounts of distortional strain on the dioxazolone during the carbon dioxide removal step.

The dioxazolone fragments from the rhodium and iridium cases are shown below in Figure 16, with both the N-O-O angle and the N-O distance highlighted. As is evident from the figure, the dioxazolone fragment from the iridium complex has a smaller N-O-O angle and a shorter N-O distance.

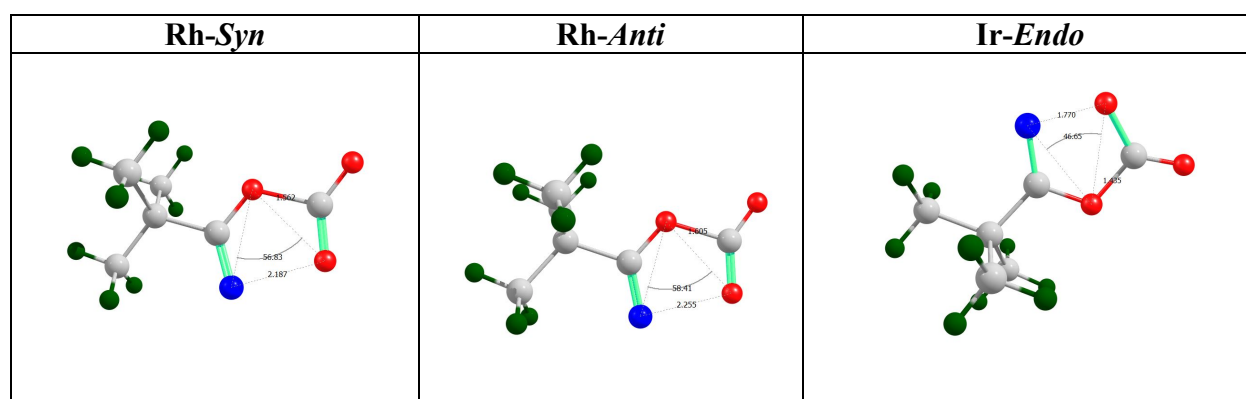


Figure 16. The distorted dioxazolone fragments that were analyzed in the distortion/interaction-activation fragment analysis described here. In all three fragments, the N-O-O angle and N-O distance (in Angstroms) are highlighted. These fragments come from the transition states for the carbon dioxide removal step of the reaction pathway for each metal center that were described in Figures 14 and 15.

According to a similar study comparing differential reactivity of Rh(III) and Ir(III) by Chang and Baik in 2016, Ir(III) experiences more relativistic contraction of its orbitals than Rh(III), which causes iridium to act as a much harder Lewis acid than rhodium.¹¹ As a result, the bond between the iridium and the nitrogen of the dioxazolone is stronger and is able to maintain more of the π -character than its counterpart in the rhodium complex. Because the bond is shorter and stronger, the overall π -conjugation from the metal center to the pivalic oxygen is better

maintained, and the fragment is better stabilized by the iridium center. Therefore, the dioxazolone fragment does not become as strained as its counterpart in the rhodium complex and exhibits both a smaller N-O-O angle and a shorter N-O distance in the transition state. The magnitude of this difference ultimately causes the reaction to prefer the opposite regioisomer of the one that is preferred in the rhodium reaction, as has been described previously.

Development of a Novel Chiral Indenylrhodium Catalyst

The indenyl-sulfoxide ligand scaffold aimed to be synthesized in this study was inspired by a similar ligand scaffold first synthesized by Trost.¹³ The modified synthetic scheme used to synthesize this ligand scaffold is shown below in Figure 17.

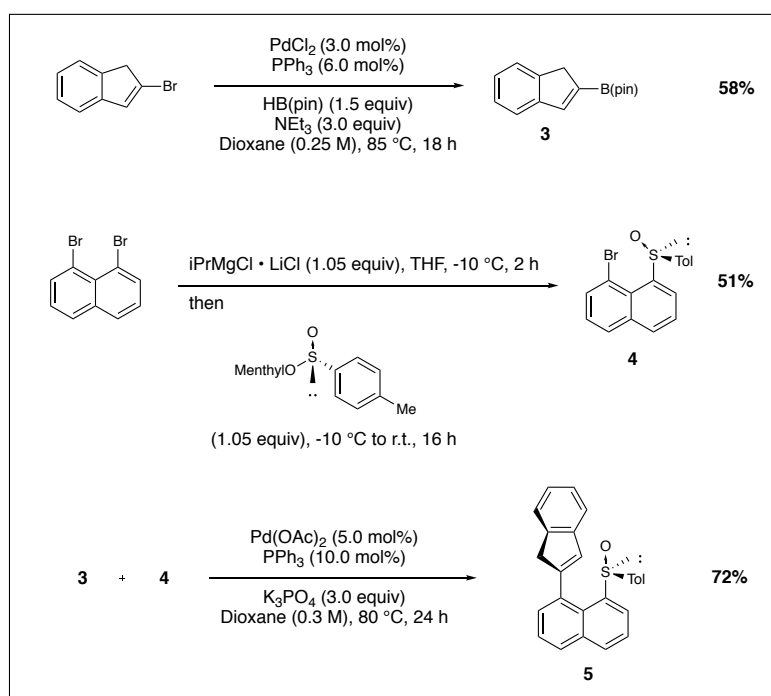


Figure 17. The synthetic scheme used to prepare the indenyl ligand scaffold used in this study. This synthetic procedure is modified from a previously published synthesis of a similar ligand scaffold that was initially done by Trost.¹³ The yields shown in the figure are the isolated yields measured from the preparation of each species in this study.

The first portion of the synthesis was the synthesis of 2-(1H-inden-2-yl)-4,4,5,5-tetramethyl-1,3,2-dioxaborolane (**3**) from Figure 17 above. Adding 3.0 mol% of PdCl₂, 6.0 mol% of PPh₃, 1.5 equivalents of HB(pin), and 3.0 equivalents of distilled triethylamine to a 0.25 M solution of 1-bromoindene in dioxane gave indenyl-pinacolborane species **3** in 58% yield. The importance of using freshly distilled triethylamine and air-free technique was noted, as the yields were substantially reduced when either of these was absent.

The second portion of the synthesis of the ligand scaffold was the synthesis of (*S*)-1-bromo-8-(*p*-tolylsulfinyl)naphthalene (**4**) from Figure 17 above. To 6.6 mL of a 0.5 M solution of 1,8-dibromonaphthalene in THF was added 2.73 mL of a 1.3 M solution of *i*PrMgCl • LiCl in THF. After stirring at -10 °C for 2 hours, 4.3 mL of a 0.8 M solution of (1*R*,2*S*,5*R*)-(-)-Menthyl (*S*)-*p*-toluenesulfinate in THF was added to the reaction vial, and the resulting solution was allowed to stir at room temperature for 16 hours to generate naphthyl species **4** in 51% yield. In the early stages of this study, this synthesis was done by manually generating the *i*PrMgCl • LiCl by stirring a solution of *i*PrMgCl with added LiCl prior to the addition of the 1,8-dibromonaphthalene. However, after several trials with unacceptably low yields, the decision was made to switch to directly adding pre-purchased *i*PrMgCl • LiCl to the 1,8-dibromonaphthalene as described here.

Finally, to complete the synthesis of the indenyl ligand scaffold, a coupling reaction between indenyl-pinacolborane species **3** and naphthyl species **4** was carried out. To a dry, air-free mixture of solid Pd(OAc)₂ (5.0 mol%), PPh₃ (10.0 mol%), K₃PO₄ (3.0 equivalents), and indenyl-pinacolborane species **3** (1.1 equivalents) was added 1.23 mL of a 0.3 M solution of naphthyl species **4** in dioxane. After allowing the reaction to stir at 80 °C for 24 hours, indenyl-sulfoxide species **5** was generated in 72% yield. Again, the importance of using dry reagents was

noted during the numerous replications of this reaction, as the yield decreased significantly when K_3PO_4 from the general storage cabinet was used as opposed to K_3PO_4 that had been pre-dried and stored in a dessicator prior to adding it to the reaction vial.

When Trost initially synthesized an analog of this indenyl-sulfoxide ligand scaffold, it was subsequently complexed to a ruthenium metal center using a photoredox method.¹³ However, the purpose of synthesizing this ligand scaffold was to complex it to rhodium. Other, less complicated methods are typically used to complex indenyl ligand scaffolds to rhodium metal centers as opposed to ruthenium, and as a result different complexation procedures were sought out.¹⁷ The first attempts at complexation were inspired by a 2012 investigation by Baker, in which several axially chiral indenyl-sulfoxide ligand scaffolds were complexed to a rhodium center using a simple reflux methodology.¹⁷ In this study, three attempts were made to complex indenyl-sulfoxide species **5** to a Rh(III) center via reflux. These attempts, which all failed, are detailed below in Figure 18.

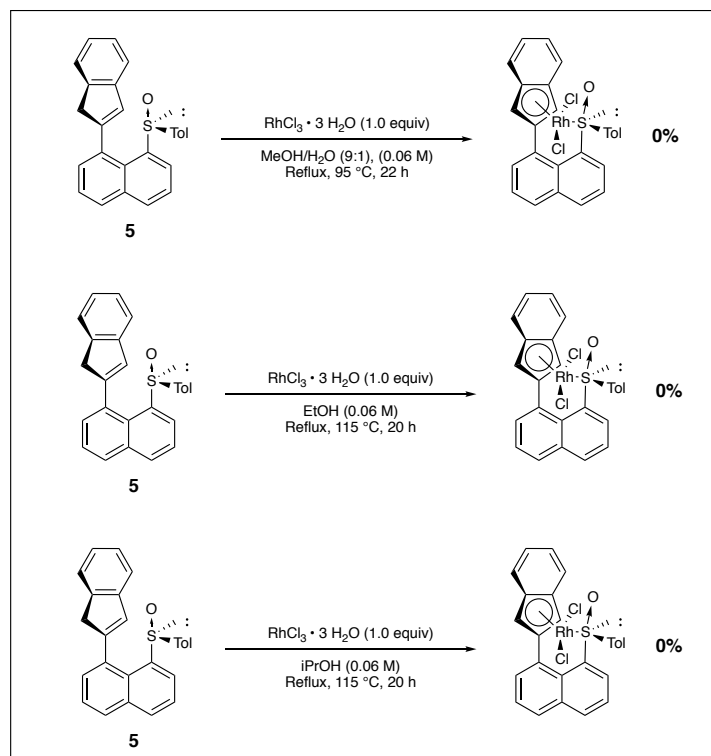


Figure 18. A depiction of the three attempts to complex ligand scaffold **5** onto a Rh(III) metal center directly by using a reflux methodology adopted from Baker.¹⁷ As is evident from the figure, all 3 attempts failed and resulted in the degradation of the ligand scaffold, according to the crude ¹H NMR spectra taken after the reflux periods indicated.

As is evident from Figure 18 above, all three attempts to form the Rh(III) complex by refluxing in an alcohol were unsuccessful. This is likely because the alcohols were not basic enough to deprotonate the indene to enable it to coordinate to the rhodium center in an η^5 fashion. Prior to using harsher reagents such as a strong base, an attempt was made to complex the indenyl-sulfoxide ligand scaffold by microwaving it at 140 °C in methanol for three minutes. This attempt, depicted below in Figure 19, also failed, and resulted in the decomposition of the indenyl-sulfoxide species **5** such that it was unrecognizable in the crude ¹H NMR spectrum.

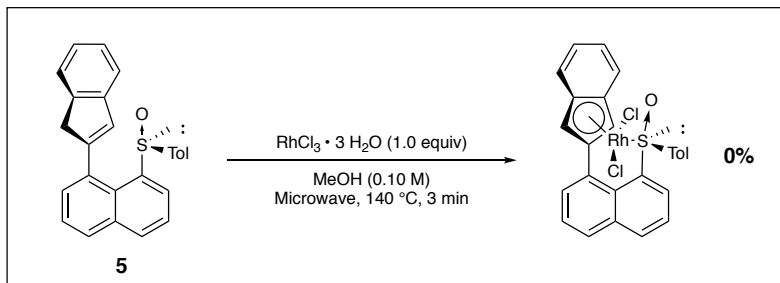


Figure 19. A schematic of the reaction conditions used for the attempt to complex ligand scaffold **5** directly onto a Rh(III) metal center using a microwave methodology. This attempt also failed and resulted in the degradation of the ligand scaffold, as was evident from the crude ^1H NMR spectrum taken after the microwave period.

Following the several failed attempts to generate the indenylrhodium (III) complex by reacting the indenyl-sulfoxide ligand scaffold with RhCl_3 in an alcohol, a transition was made to a slightly more complicated reaction setup using harsher reagents. Concurrent studies by other members of the Blakey group investigating the syntheses of various other indenylrhodium complexes demonstrated that a viable reaction setup is that depicted below in Figure 20. As is shown in the figure, the plan was to complex the indenyl-sulfoxide ligand scaffold to a Rh(I) center using $\text{KO}t\text{Bu}$ as a strong base, and oxidize the resulting Rh(I) complex to a Rh(III)-diiodide dimer using solid I_2 crystals.

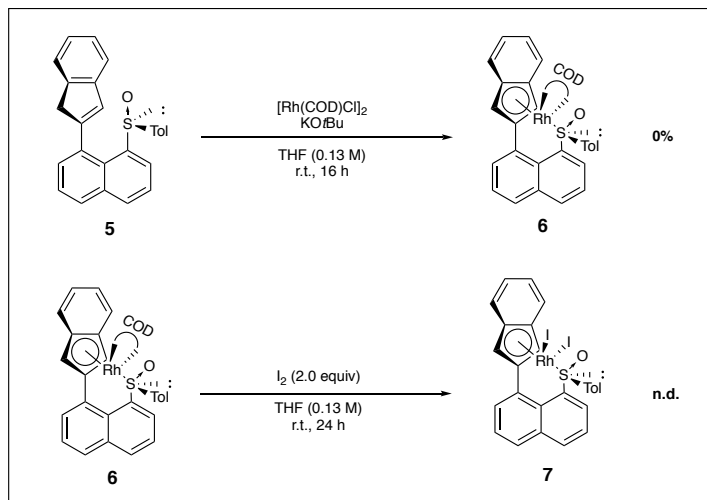


Figure 20. The synthetic scheme used to complex the indenyl ligand scaffold **5** to a Rh(I) metal center prior to oxidation to the Rh(III) dimer using solid iodine crystals. Analysis of the first reaction (to form species **6**) is ongoing to determine if the synthetic scheme is viable.

To generate the Rh(I) complex, the reaction scheme detailed in Figure 20 above was carried out. To a dry, air-free mixture of solid indenyl-sulfoxide species **5** (2.1 equivalents), KOtBu (2.5 equivalents), and $[\text{Rh}(\text{COD})\text{Cl}]_2$ (1.0 equivalent) was added 0.5 mL of dry THF. The resulting solution was briefly sonicated and allowed to stir at room temperature for 16 hours, giving what appeared to be indenylrhodium (I) complex **6** in approximately quantitative yield, according to the ^1H NMR. However, in the process of collecting standard characterization data, mass spectrometry was performed on what was thought to be complex **6**, and the expected m/z peak could not be located in the resulting mass spectrum. This is indicative of the possible failure of indenyl-sulfoxide species **5** to complex onto the rhodium metal center as schematized above. The product that was analyzed by ^1H NMR and mass spectrometry was a brilliant yellow powder, which is consistent with the color of cyclooctadienylrhodium (I) complexes including the one that was used as a reagent in this reaction, and the ^1H NMR spectrum appeared to be very similar to the purified indenyl-sulfoxide species **5**, which indicates that the ligand scaffold was likely not destroyed over the course of this reaction. However, further analysis is needed to

determine exactly what was formed in this reaction, and the process of further analyzing this crude reaction mixture is ongoing.

When indenylrhodium (I) complex **6** is successfully synthesized, the next step will be to oxidize it to obtain the desired indenylrhodium (III) diiodide dimer complex **7**. This will ideally be done by dissolving it in THF with 2.0 equivalents of solid I₂ crystals, which should dislodge the COD ligand and replace it with one iodide anion and one bridging iodine (to form the scaffold of the dimer) per rhodium center.

The purpose for the development of a viable synthetic scheme for complex **7** is to be able to reliably synthesize this complex to examine its potential catalytic utility in regio- and enantioselective allylic C-H functionalization reactions. Unfortunately, due to the large amount of time it has taken to devise the still incomplete synthetic scheme described in this section, these investigations of catalytic utility are still in their nascent stages. However, preliminary results from the application of similar indenylrhodium complexes to allylic C-H functionalization reactions in the Blakey group have indicated promising results with very high enantioselectivities.¹⁶ Ideally, this complex will also be able to enantioselectively catalyze a suite of allylic C-H functionalization reactions, which would encourage a future investigation into alterations of the sulfoxide portion of the ligand scaffold to further fine-tune the reactivity of the complex.

Conclusions and Future Directions: Although the intensive investigation into allylic C-H alkylation with malonate-derivative carbon nucleophiles was met with mixed success, it was valuable in context because it expanded upon the scope of compatible nucleophiles for Group IX metal-catalyzed allylic C-H functionalization reactions. As is evident from the data provided

here, approximately half of the nucleophile scope proved to be incompatible with the reaction conditions developed in this study. However, the approximately half that were tolerated demonstrated that malonate-derivative carbon nucleophiles with polar yet relatively resistant-to-modification functional groups (e.g. esters, ketones, and nitro groups) are promising candidates for implementation in future syntheses using this method. By expanding the scope of compatible nucleophiles that can be used in this methodology, this study has provided further support for the widespread adoption of Group IX metal-catalyzed allylic C-H functionalization in higher stakes, pharmaceutically relevant syntheses.

The computational study to elucidate the origins of the observed regioselectivity difference between isoelectronic Rh(III) and Ir(III) with identical ligand scaffolds was significant. This is because it highlighted physicochemical differences between these two Group IX metals that will enable future organometallic chemists to make informed decisions to fine-tune the regioselectivity of their reactions. Although this study was limited to the allylic C-H amidation reactions published by Blakey in 2019, the data produced here corroborate other studies as was previously discussed. In these studies, the same concept was emphasized: that the differences in the relativistic contraction between rhodium and iridium have significant implications for reactivity and may cause otherwise identical rhodium and iridium complexes to yield completely different products in the same general catalytic organometallic reactions. The broad applicability of the relativistic differences between rhodium and iridium are promising for future methodology development as organometallic chemists continue to expand the area of regioselective C-H functionalization.

The elucidation of a robust synthetic scheme for the indenyl-sulfoxide rhodium (III) complex would represent an advance on the current cutting edge of enantioselective C-H

functionalization chemistry. To date, very few rhodium complexes with indenyl ligand scaffolds have been synthesized, and even fewer have been investigated in the context of C-H functionalization chemistry. The successful synthesis of such a complex with an indenyl-sulfoxide ligand scaffold will open a new avenue of future investigations into catalyst development by establishing precedent for a complex with a modifiable sulfoxide functional group. While the ability of this complex to effectively regio- and enantioselectively catalyze allylic C-H functionalization reactions is still the subject of intense study, the fact that other indenylrhodium complexes have been able to enantioselectively catalyze allylic C-H functionalization reactions is promising. Ideally, future studies will indicate that this complex is also a viable catalyst for a variety of enantioselective C-H functionalization reactions, and further studies into modifications to fine-tune its catalytic activity will be warranted.

Supplemental Information

General Information

Materials: All reagents were purchased from commercial sources (Alfa Aesar, Fischer Scientific, Fluka, Oakwood, and Sigma Aldrich) and were used as received unless otherwise specified.

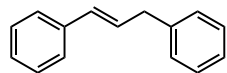
Dichloroethane was purified via distillation over calcium hydride, while all other anhydrous solvents were purified through alumina using a Glass Contours solvent purification system.

Solvents utilized in reaction workup and flash chromatography procedures were used as received from commercial suppliers without further purification measures. All reaction setups and solution preparations were performed using anhydrous solvents in oven-dried glassware that had been charged with nitrogen gas using Schlenk technique.

Analysis: ^1H and ^{13}C NMR spectra were taken on either a Mercury 300 PLUS spectrometer (300 MHz ^1H , 75 MHz ^{13}C), Varian Inova 500 spectrometer (500 MHz ^1H , 125 MHz ^{13}C), Varian Inova 400 spectrometer (400 MHz ^1H , 100 MHz ^{13}C), or Varian VNMRS 400 spectrometer (400 MHz ^1H , 100 MHz ^{13}C) at room temperature in CDCl_3 that had been neutralized and dried using anhydrous K_2CO_3 with internal CHCl_3 as the reference (7.26 ppm for ^1H and 77.16 ppm for ^{13}C), unless otherwise specified. Chemical shift values (δ) were reported in parts per million (ppm) and coupling constants (J-values) were reported in Hertz (Hz). Multiplicity was indicated using the following abbreviations: s = singlet, d = doublet, t = triplet, q = quartet, and m = multiplet. Infrared (IR) absorption spectra were taken using a Thermo Electron Corporation Nicolet 380 FT-IR spectrometer. High-resolution mass spectra were taken using a Thermo Electron Corporation Finigan LTQFTMS spectrometer at the Mass Spectrometry Facility of Emory University. Analytical thin layer chromatography (TLC) was done on pre-coated, glass-backed EMD 0.25 mm silica gel 60 plates. The plates were visualized using short- or long-wave UV light in combination with the following stains: *p*-anisaldehyde, KMnO_4 , Cerium Ammonium Molybdate (CAM), or Phosphomolybdic Acid. Flash column chromatography was done using Silicycle SilaFlash F60 silica gel (40-63 μm).

Materials Preparation

1,3-*trans*-diphenylpropene



Into a 500 mL round-bottom flask charged with a magnetic stir bar were added phenylacetaldehyde (4.0 g, 33.29 mmol) and potassium hydroxide pellets (28.4 g, 506.15 mmol). After adding the reagents, ethanol (234 mL) was added to dissolve them. The resulting mixture

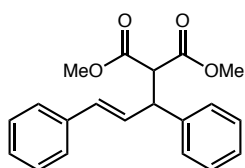
was heated to 95 °C, stirred, and allowed to reflux for 24 hours. After 24 hours, the mixture was cooled to room temperature and concentrated under reduced pressure before being re-dissolved in 100 mL of distilled water and extracted three times with diethyl ether. The organic layers were combined, washed with brine, and dried over magnesium sulfate. The crude reaction mixture was purified via flash chromatography on silica gel using a gradient of hexanes and diethyl ether to give a light-yellow oil (1.45 g, 45% yield). The compound exhibited identical ^1H NMR data to previous reports. ^1H NMR (400 MHz, CDCl_3): δ 7.36-7.17 (m, 10H), 6.45 (d, $J = 15.8$ Hz, 1H), 6.35 (dt, $J = 15.7, 6.6$ Hz, 1H), 3.54 (d, $J = 6.5$ Hz, 1H) ppm.

Procedure for the Optimization of Allylic C-H Alkylation with Dimethyl Malonate

Inside an N_2 -filled glovebox, an oven-dried 7 mL vial was charged with the designated amounts of $[\text{RhCp}^*\text{Cl}_2]_2$, silver acetate, and silver hexafluoroantimonate, along with a magnetic stir bar. Following the addition of the solids, the vial was sealed with a Teflon septum cap and removed from the glovebox. In a separate oven-dried 7 mL vial sealed with a Teflon septum cap, a 0.40 M solution of 1,3-*trans*-diphenylpropene was prepared in anhydrous 1,2-dichloroethane under an inert N_2 atmosphere using Schlenk technique. Prior to the evacuation of the atmosphere, 0.25 equivalents of 1,4-dinitrobenzene were added as the internal standard to monitor the reaction by ^1H NMR. In a third separate oven-dried 7 mL vial sealed with a Teflon septum cap, a solution of 1.5 times the necessary molar equivalents of dimethyl malonate was prepared in 1,2-dichloroethane under an inert N_2 atmosphere using Schlenk technique. Following the preparation of the two reagent solutions, 1 mL of each was added to the initial 7 mL reaction vial containing the solids that had been weighed out in the glovebox. After combining the contents of the three vials as described, the inert N_2 atmosphere was maintained in the reaction vial using an N_2 -filled

balloon. The reaction vial was heated to the desired temperature and after the designated amount of time, the reaction vial was opened to air and allowed to cool to room temperature. The contents of the reaction vial were filtered through a pipet plug of celite, which was then rinsed with 15 mL of dichloromethane. The filtrate was concentrated under reduced pressure and analyzed by ^1H NMR.

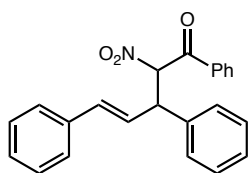
Dimethyl (*E*)-2-(1,3-diphenylallyl)malonate (**2a**)



Inside an N_2 -filled glovebox, an oven-dried 7 mL vial was charged with silver hexafluoroantimonate (12.0 mg, 0.035 mmol), silver acetate (140.1 mg, 0.84 mmol), $[\text{RhCp}^*\text{Cl}_2]_2$ (5.0 mg, 0.0081 mmol), and a magnetic stir bar. Following the addition of the solids to the vial, it was sealed with a Teflon septum cap and removed from the glovebox. In a separate oven-dried 7 mL vial sealed with a Teflon septum cap, a solution of 1,3-*trans*-diphenylpropene (113.7 mg, 0.59 mmol) was prepared in anhydrous 1,2-dichloroethane (1.48 mL) under an inert N_2 atmosphere using Schlenk technique. In a third oven-dried 7 mL vial sealed with a Teflon septum cap, a solution of dimethyl malonate (130.79 mg, 0.113 mL, 0.99 mmol) was prepared in anhydrous 1,2-dichloroethane (1.50 mL) under an inert N_2 atmosphere using Schlenk technique. Following the preparation of these reagent solutions, a 1 mL aliquot of each was transferred to the initial 7 mL reaction vial containing the solids from the glovebox. The resulting mixture was heated to 80 $^\circ\text{C}$ and stirred for 24 hours under an inert N_2 atmosphere maintained by an N_2 -filled balloon. The reaction mixture was then cooled to room temperature and opened to air before being filtered over a pipet plug of celite. The celite was rinsed with 15 mL of dichloromethane,

and the combined filtrate was concentrated under reduced pressure. The crude reaction mixture was then purified via flash chromatography on silica gel using a gradient of Toluene:Et₂O (98:2 → 95:5) to give the title compound as a viscous yellow oil (82.4 mg, 64% yield). The compound exhibited identical ¹H NMR data to previous reports. **¹H NMR** (400 MHz, CDCl₃): δ 7.34-7.18 (m, 10H), 6.48 (d, J = 15.78 Hz, 1H), 6.33 (dd, J = 15.70, 8.58 Hz, 1H), 4.27 (dd, J = 10.87, 8.63 Hz, 1H), 3.95 (d, J = 10.92 Hz, 1H), 3.71 (s, 3H), 3.52 (s, 3H) ppm.

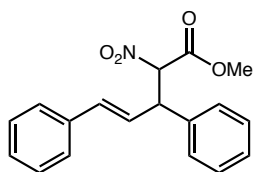
(E)-2-nitro-1,3,5-triphenylpent-4-en-1-one (2b)



Inside an N₂-filled glovebox, an oven-dried 7 mL vial was charged with silver hexafluoroantimonate (9.0 mg, 0.026 mmol), silver acetate (95.6 mg, 0.57 mmol), [RhCp*Cl₂]₂ (3.2 mg, 0.0052 mmol), and a magnetic stir bar. Following the addition of the solids to the vial, it was sealed with a Teflon septum cap and removed from the glovebox. In a separate oven-dried 7 mL vial sealed with a Teflon septum cap, a solution of 1,3-*trans*-diphenylpropene (77.3 mg, 0.40 mmol) was prepared in anhydrous 1,2-dichloroethane (1.07 mL) under an inert N₂ atmosphere using Schlenk technique. In a third oven-dried 7 mL vial sealed with a Teflon septum cap, a solution of benzoylnitromethane (176.7 mg, 1.07 mmol) was prepared in anhydrous 1,2-dichloroethane (1.07 mL) under an inert N₂ atmosphere using Schlenk technique. Following the preparation of these reagent solutions, a 1 mL aliquot of each was transferred to the initial 7 mL reaction vial containing the solids from the glovebox. The resulting mixture was heated to 80 °C and stirred for 24 hours under an inert N₂ atmosphere maintained by an N₂-filled balloon. The reaction mixture was then cooled to room temperature and opened to air before being filtered

over a pipet plug of celite. The celite was rinsed with 15 mL of dichloromethane, and the combined filtrate was concentrated under reduced pressure. The crude reaction mixture was then purified via flash chromatography on silica gel using a gradient of Toluene:Et₂O (98:2 → 95:5) to give the title compound as a viscous yellow oil (88.8 mg, 97% yield) in a 1:1 mixture of two diastereomers. **Rf** = 0.78 in 95:5 Toluene:Et₂O. **¹H NMR** (500 MHz, CDCl₃): δ 8.04 (d, J = 7.34 Hz, 2H), 7.84 (d, J = 7.35 Hz, 2H), 7.65-7.05 (m, 26H), 6.60 (dd, J = 15.8, 10.8 Hz, 2 H), 6.41 (td, J = 15.7, 4.8 Hz, 2 H), 6.05 (dd, J = 15.7, 8.5 Hz, 2H), 4.77 (m, 2H) ppm. **¹³C NMR** (125 Hz, CDCl₃): δ 187.5, 186.8, 137.6, 136.8, 136.2, 136.1, 134.9, 134.7, 134.5, 134.4, 133.9, 129.2, 129.1, 129.09, 129.04, 128.97, 128.8, 128.5, 128.4, 128.3, 127.99, 127.94, 127.75, 126.6, 126.3, 125.8, 125.2, 91.4, 90.9, 50.45, 50.3 ppm. **HRMS** (+ p NSI): Calculated for C₂₃H₁₉NO₃ [M+Na]⁺ 380.12571, observed 380.12562. **IR** (thin film): 3061, 3029, 1694, 1652, 1554, 1358, 693 cm⁻¹.

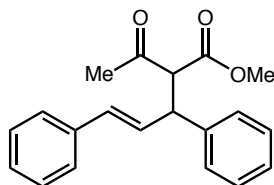
Methyl (*E*)-2-nitro-3,5-diphenylpent-4-enoate (2c)



Inside an N₂-filled glovebox, an oven-dried 7 mL vial was charged with silver hexafluoroantimonate (5.5 mg, 0.016 mmol), silver acetate (70.0 mg, 0.42 mmol), [RhCp*Cl₂]₂ (3.1 mg, 0.0050 mmol), and a magnetic stir bar. Following the addition of the solids to the vial, it was sealed with a Teflon septum cap and removed from the glovebox. In a separate oven-dried 7 mL vial sealed with a Teflon septum cap, a solution of 1,3-*trans*-diphenylpropene (117 mg, 0.60 mmol) and methyl nitroacetate (0.28 mL, 3.0 mmol) was prepared in dichloromethane (3.0 mL) under an inert N₂ atmosphere using Schlenk technique. A 1 mL aliquot of this solution was

transferred to the 7 mL reaction vial containing the solids from the glovebox. The resulting mixture was heated to 80 °C and stirred for 24 hours under an inert N₂ atmosphere maintained by an N₂-filled balloon. The reaction mixture was then cooled to room temperature and opened to air before being filtered over a pipet plug of celite. The celite was rinsed with 7 mL of ethyl acetate, and the combined filtrate was concentrated under reduced pressure. The crude reaction mixture was then purified via flash chromatography on silica gel using a gradient of Hexanes:EtOAc (95:5 → 0:100) to give the title compound as a yellow oil (48 mg, 76% yield) in a 1:1 mixture of two diastereomers. **Rf** = 0.32 in 85:15 Hexanes:EtOAc. **¹H NMR** (500 MHz, CDCl₃): δ 7.37-7.23 (m, 20H), 6.56 (d, J = 15.7 Hz, 2H), 6.38 (dd, J = 15.7, 8.7 Hz, 1H), 6.25 (dd, J = 15.7, 9.0 Hz, 1H), 5.55 (t, J = 11.0 Hz, 2H), 4.52 (dt, J = 20.5, 10.1 Hz, 2H), 3.79 (s, 3H), 3.61 (s, 3H) ppm. **¹³C NMR** (125 MHz, CDCl₃): δ 163.7, 163.2, 137.3, 136.7, 136.1, 129.2, 129.1, 128.6, 128.5, 128.2, 128.1, 128.09, 128.07, 128.06, 127.7, 126.6, 126.5, 125.3, 124.9, 91.7, 91.2, 53.6, 53.4, 50.5, 50.3, 29.7 ppm. **HRMS** (+ p NSI): Calculated for C₁₈H₁₇NO₄ [M+Na]⁺ 334.10510, observed 334.10498. **IR** (thin film): 2923, 2853, 1751, 1558, 743, 694 cm⁻¹.

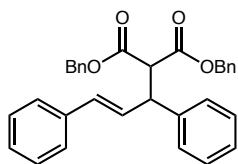
Methyl (*E*)-2-acetyl-3,5-diphenylpent-4-enoate (2d)



Inside an N₂-filled glovebox, an oven-dried 7 mL vial was charged with silver hexafluoroantimonate (5.5 mg, 0.016 mmol), silver acetate (70.0 mg, 0.42 mmol), [RhCp*Cl₂]₂ (2.5 mg, 0.004 mmol), and a magnetic stir bar. Following the addition of the solids to the vial, it

was sealed with a Teflon septum cap and removed from the glovebox. In a separate oven-dried 7 mL vial sealed with a Teflon septum cap, a solution of 1,3-*trans*-diphenylpropene (117 mg, 0.60 mmol) and methyl acetoacetate (0.03 mL, 0.30 mmol) was prepared in dichloromethane (1.5 mL) under an inert N₂ atmosphere using Schlenk technique. A 1 mL aliquot of this solution was transferred to the 7 mL reaction vial containing the solids from the glovebox. The resulting mixture was heated to 80 °C and stirred for 24 hours under an inert N₂ atmosphere maintained by an N₂-filled balloon. The reaction mixture was then cooled to room temperature and opened to air before being filtered over a pipet plug of celite. The celite was rinsed with 7 mL of ethyl acetate, and the combined filtrate was concentrated under reduced pressure. The crude reaction mixture was then purified via flash chromatography on silica gel using a gradient of Hexanes:EtOAc (97:3 → 80:20) to give the title compound as a yellow oil (53 mg, 87% yield) in a 1:1 mixture of two diastereomers. The compound exhibited identical ¹H NMR data to previous reports. **Rf** = 0.22 in 9:1 Hexanes:EtOAc. **¹H NMR** (400 MHz, CDCl₃): δ 7.32-7.18 (m, 20H), 6.45 (d, J = 11.9 Hz, 1H), 6.41 (d, J = 11.9 Hz, 1H), 6.27 (dd, J = 13.0, 5.6 Hz, 1H), 6.22 (dd, J = 13.0, 5.6 Hz, 1H), 4.28 (dd, J = 8.3, 3.0 Hz, 1H), 4.26 (dd, J = 8.3, 3.0 Hz, 1H), 4.11 (d, J = 9.6 Hz, 1H), 4.08 (d, J = 9.6 Hz, 1H), 3.67 (s, 3H), 3.47 (s, 3H), 2.28 (s, 3H), 2.01 (s, 3H) ppm.

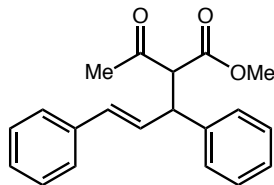
Dibenzyl (*E*)-2-(1,3-diphenylallyl)malonate (**2e**)



Inside an N₂-filled glovebox, an oven-dried 7 mL vial was charged with silver hexafluoroantimonate (7.1 mg, 0.021 mmol), silver acetate (90.1 mg, 0.54 mmol), [RhCp*Cl₂]₂ (3.2 mg, 0.0052 mmol), and a magnetic stir bar. Following the addition of the solids to the vial, it

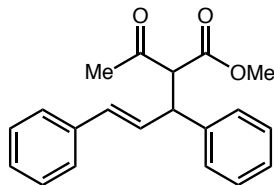
was sealed with a Teflon septum cap and removed from the glovebox. In a separate oven-dried 7 mL vial sealed with a Teflon septum cap, a solution of 1,3-*trans*-diphenylpropene (88.9 mg, 0.46 mmol) was prepared in anhydrous 1,2-dichloroethane (1.14 mL) under an inert N₂ atmosphere using Schlenk technique. In a third oven-dried 7 mL vial sealed with a Teflon septum cap, a solution of dibenzyl malonate (274.0 mg, 0.96 mmol) was prepared in anhydrous 1,2-dichloroethane (0.96 mL) under an inert N₂ atmosphere using Schlenk technique. Following the preparation of these reagent solutions, a 0.64 mL aliquot of each was transferred to the initial 7 mL reaction vial containing the solids from the glovebox. The resulting mixture was heated to 80 °C and stirred for 24 hours under an inert N₂ atmosphere maintained by an N₂-filled balloon. The reaction mixture was then cooled to room temperature and opened to air before being filtered over a pipet plug of celite. The celite was rinsed with 15 mL of dichloromethane, and the combined filtrate was concentrated under reduced pressure. The crude reaction mixture was then purified via flash chromatography on silica gel using a gradient of Hexanes:Et₂O:Toluene (95:0:5 → 80:15:5) to give the title compound as a viscous yellow oil (9.4 mg, <7% yield). **Rf** = 0.62 in 80:15:5 Hexanes:Et₂O:Toluene. The compound exhibited identical ¹H NMR data to previous reports. **¹H NMR** (400 MHz, CDCl₃): δ 7.30-7.18 (m, 28H), 7.05-7.01 (m, 2H), 6.41 (d, J = 15.8 Hz, 1H), 6.29 (dd, J = 15.8, 7.9 Hz, 1H), 5.09 (dd, J = 12.0, 13.9 Hz, 2H), 4.91 (dd, J = 12.1, 14.0 Hz, 2H), 4.28 (dd, J = 8.3, 10.8 Hz, 1H), 4.03 (d, J = 10.9 Hz, 1H) ppm.

Procedure for the Rhodium Mechanistic Study

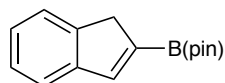


Inside an N₂-filled glovebox, an oven-dried 7 mL vial was charged with a magnetic stir bar and [RhCp*(CH₃CN)₃](SbF₆)₂ (6.7 mg, 0.008 mmol). The vial was then sealed with a Teflon septum cap and removed from the glovebox. In a separate oven-dried 7 mL vial sealed with a Teflon septum cap, a solution of 1,3-*trans*-diphenylallyl acetate (76 mg, 0.30 mmol) and dimethyl malonate (0.086 mL, 0.75 mmol) was prepared in dichloromethane (1.5 mL) under an inert N₂ atmosphere using Schlenk technique. A 1 mL aliquot of this solution was transferred to the initial 7 mL vial containing the solids from the glovebox, which was kept under an inert N₂ atmosphere using an N₂-filled balloon. The resulting mixture was heated to 80 °C and allowed to stir for 24 hours. The crude reaction mixture was then cooled to room temperature and filtered over a pipet plug of celite. The celite was then rinsed with 7 mL of ethyl acetate, and the combined filtrate was concentrated under reduced pressure. The crude reaction mixture was then purified by flash chromatography on silica gel using a gradient of Toluene:Et₂O (98:2 → 95:5) to provide the title compound as a viscous yellow oil (43 mg, 66% yield). The compound exhibited identical ¹H NMR data to previous reports.

Procedure for the Silver Mechanistic Study



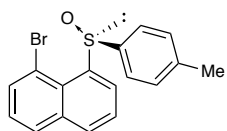
Inside an N₂-filled glovebox, an oven-dried 7 mL vial was charged with a magnetic stir bar and silver hexafluoroantimonate (2.3 mg, 0.0067 mmol). The vial was then sealed with a Teflon septum cap and removed from the glovebox. In a separate oven-dried 7 mL vial sealed with a Teflon septum cap, a solution of 1,3-*trans*-diphenylallyl acetate (86.0 mg, 0.34 mmol) was prepared in anhydrous 1,2-dichloroethane (0.86 mL) under an inert N₂ atmosphere using Schlenk technique. In a third oven-dried 7 mL vial sealed with a Teflon septum cap, a solution of dimethyl malonate (99.2 mg, 0.09 mL, 0.75 mmol) was prepared in anhydrous 1,2-dichloroethane (0.75 mL). Following the preparation of the reagent solutions, a 0.5 mL aliquot of each was taken and added to the initial 7 mL vial with the solids from the glovebox. The resulting mixture was heated to 80 °C and allowed to stir for 24 hours under an inert N₂ atmosphere maintained by an N₂-filled balloon. The reaction mixture was then cooled to room temperature and opened to air before being filtered through a pipet plug of celite. The celite was then rinsed with 15 mL of dichloromethane and the combined filtrate was concentrated under reduced pressure. The crude reaction mixture was then purified via flash chromatography on silica gel using a gradient of Toluene:Et₂O (98:2 → 95:5) to provide the title compound as a viscous yellow oil (28 mg, 43% yield). The compound exhibited identical ¹H NMR data to previous reports.

2-(1H-inden-2-yl)-4,4,5,5-tetramethyl-1,3,2-dioxaborolane (3)

Inside an N₂-filled glovebox, an oven-dried 50 mL round-bottomed flask was charged with PdCl₂ (28.2 mg, 0.16 mmol), PPh₃ (80.6 mg, 0.31 mmol), and a magnetic stir bar. The flask was sealed with a rubber septum and removed from the glovebox. After being removed from the glovebox, the flask was kept under an inert N₂ atmosphere maintained by an N₂-filled balloon. After installing the N₂-filled balloon, pre-distilled triethylamine (1.56 g, 2.15 mL, 15.4 mmol) was added to the flask via syringe under air-free conditions using Schlenk technique. In a separate oven-dried 50 mL round-bottomed flask sealed with a rubber septum, a solution of 2-bromoindene (1147 mg, 5.88 mmol) was prepared in anhydrous 1,4-dioxane (23.6 mL). Prior to adding the dioxane, the solid 2-bromoindene was put into the flask, and the atmosphere was evacuated and backfilled with inert N₂ gas three times using Schlenk technique to ensure air-free conditions. After briefly sonicating this flask to ensure homogenization of the 2-bromoindene in the dioxane, 20.6 mL of the 2-bromoindene solution was transferred via syringe to the initial flask containing the solids from the glovebox. After adding the 2-bromoindene solution, the N₂-filled balloon was temporarily removed and the reaction flask was sparged with N₂ gas for 15 minutes. The N₂-filled balloon was then re-equipped onto the reaction flask and liquid 4,4,5,5-tetramethyl-1,3,2-dioxaborolane (985 mg, 1.12 mL, 7.70 mmol) was carefully added dropwise to mitigate the effect of gas evolution. The resulting reaction mixture was then heated to 85 °C and allowed to stir for 18 hours. The reaction mixture was then opened to air and allowed to cool to room temperature before being transferred to a 250 mL round-bottomed flask and quenched with approximately 100 mL of brine. The resulting aqueous mixture was extracted three times with approximately 50 mL of diethyl ether. The organic layers were combined and dried over

magnesium sulfate. The crude reaction mixture was purified via flash chromatography on silica gel using a gradient of Hexanes:Et₂O (100:0 → 95:5) to provide the title compound as an off-white powder (718 mg, 58% yield). The compound exhibited identical ¹H NMR data to previous reports. ¹H NMR (400 MHz, CDCl₃): δ 7.57 (td, J = 2.01, 0.76 Hz, 1H), 7.51-7.45 (m, 2H), 7.28-7.22 (m, 2H), 3.54 (s, 2H), 1.33 (s, 12H) ppm.

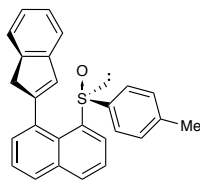
(S)-1-bromo-8-(*p*-tolylsulfinyl)naphthalene (4)



Solid 1,8-dibromonaphthalene (1044 mg, 3.65 mmol) was weighed into an oven-dried 25 mL round-bottomed flask. The flask was sealed with a rubber septum, and the atmosphere was then evacuated and backfilled with inert N₂ gas three times using Schlenk technique to ensure air-free conditions. Anhydrous tetrahydrofuran (7.3 mL) was added to the flask via syringe. A separate 25 mL round-bottomed flask was charged with a magnetic stir bar, sealed with a rubber septum, and flame-dried. This flask was then charged with an inert N₂ atmosphere which was maintained by an N₂-filled balloon. A 6.6 mL aliquot of the initial 1,8-dibromonaphthalene solution was added to the flame-dried flask via syringe, and the flask was then cooled to -10 °C using a brine/ice bath. A commercially available, pre-made solution of *i*PrMgCl • LiCl (2.73 mL of a 1.3 M solution in THF, 3.55 mmol) was then added to the flask, and the resulting mixture was allowed to stir at -10 °C for 2 hours. While this mixture was stirring, in an oven-dried 7 mL vial sealed with a Teflon septum cap, a solution of (1*R*,2*S*,5*R*)-(-)-Menthyl (*S*)-*p*-toluenesulfinate (1155 mg, 3.92 mmol) was prepared in anhydrous THF (4.9 mL). Prior to adding the THF, the sealed vial containing the toluenesulfinate had been evacuated and backfilled three times with

inert N₂ gas to ensure air-free conditions. After adding the THF, this vial was briefly sonicated to ensure complete homogenization of the toluenesulfinate in solution. Following the two hours of stirring the initial round-bottomed flask containing the 1,8-dibromonaphthalene at -10 °C, a 4.3 mL aliquot of the toluenesulfinate solution was added to the reaction mixture via syringe, and the resulting mixture was allowed to warm up to room temperature. This reaction mixture was allowed to stir for 16 hours at room temperature. The crude reaction mixture was then quenched with approximately 7 mL of saturated ammonium chloride solution. This aqueous mixture was then washed three times with diethyl ether. The organic layers were combined and dried over magnesium sulfate. The crude reaction mixture was purified via flash chromatography on silica gel using a mixture of Hexanes:EtOAc (2:1) to provide the title compound as a white crystalline solid (600 mg, 51% yield). **¹H NMR** (500 MHz, CDCl₃): δ 8.75 (dd, J = 7.52, 1.14 Hz, 1H), 8.00 (dd, J = 8.06, 1.30 Hz, 1H), 7.92 (dd, J = 8.13, 1.14 Hz, 1H), 7.83 (dd, J = 7.49, 1.18 Hz, 1H), 7.75 (t, J = 7.78 Hz, 1H), 7.41-7.39 (m, 2H), 7.35 (t, J = 7.81 Hz, 1H), 7.14-7.12 (m, 2H), 2.29 (s, 3H) ppm. **¹³C NMR** (125 MHz, CDCl₃): δ 144.9, 144.5, 141.2, 136.7, 134.4, 132.7, 129.9, 129.7, 129.4, 127.0, 126.9, 126.6, 126.3, 125.9, 117.8, 110.1, 21.5 ppm. **HRMS** (+ p NSI): Calculated for C₁₇H₁₃SOBr [M+H]⁺ 346.26146, observed 346.99257.

1-(1H-inden-2-yl)-8-(*p*-tolylsulfinyl)naphthalene (5)



Inside an N₂-filled glovebox, an oven-dried 4 mL vial was charged with a magnetic stir bar, Pd(OAc)₂ (7.5 mg, 0.033 mmol), and PPh₃ (11.3 mg, 0.043 mmol). The vial was sealed with a

Teflon septum cap and removed from the glovebox. Then, the vial was briefly opened to air, and K_3PO_4 (246.3 mg, 1.16 mmol) that had been previously dried and stored in a dessicator, and 2-(1H-inden-2-yl)-4,4,5,5-tetramethyl-1,3,2-dioxaborolane (**3**) (105.4 mg, 0.44 mmol) were quickly added to the vial. The vial was re-sealed with the Teflon septum cap, and the atmosphere was evacuated and backfilled with inert N_2 gas three times using Schlenk technique to ensure air-free conditions. The inert N_2 atmosphere was then maintained with an N_2 -filled balloon. In a separate oven-dried 7 mL vial sealed with a Teflon septum cap, a solution of (*S*)-1-bromo-8-(*p*-tolylsulfinyl)naphthalene (**4**) (600 mg, 1.68 mmol) was prepared in anhydrous 1,4-dioxane (5.6 mL). Prior to adding the dioxane, the vial containing the solid bromonaphthalene was evacuated and backfilled three times with inert N_2 gas using Schlenk technique to ensure air-free conditions. After adding the dioxane, the solution was briefly sonicated to ensure complete homogenization of the bromonaphthalene. A 1.23 mL aliquot of the bromonaphthalene solution in dioxane was added to the initial 4 mL vial containing the solids from the glovebox via syringe. The N_2 -filled balloon was temporarily removed, and the resulting mixture was sparged with N_2 gas for 15 minutes. The N_2 -filled balloon was then re-equipped onto the reaction vial, which was subsequently heated to 80 °C and allowed to stir for 24 hours. The reaction mixture was then opened to air and allowed to cool to room temperature before being filtered through a pipet plug of silica with approximately 10 mL of diethyl ether. The filtrate was concentrated under reduced pressure, and the crude reaction mixture was then purified via flash chromatography on silica gel using a mixture of Hexanes:EtOAc (4:1) to provide the title compound as a viscous, light brown oil (101 mg, 72% yield). 1H NMR (400 MHz, $CDCl_3$): δ 8.76-8.74 (m, 1H), 8.65-8.49 (br, 1H) 8.10-8.08 (m, 1H), 8.01-7.99 (m, 1H), 7.95-7.91 (m, 1H), 7.84-7.82 (m, 1H), 7.78-7.73 (m, 1H), 7.53-7.50 (m, 1H), 7.41-7.32 (m, 2H), 7.29-7.27 (m, 1H), 7.14-7.11 (m, 1H), 7.08-6.84 (br, 2H),

6.38-6.17 (br, 1H), 4.21-4.00 (br, 1H), 3.67-3.27 (br, 1H), 2.29 (s, 3H) ppm. ^{13}C NMR (125 MHz, CDCl_3): δ 146.0, 144.5, 144.1, 143.3, 132.7, 131.6, 130.3, 130.1, 130.0, 129.9, 129.7, 129.5, 128.5, 128.4, 127.7, 126.8, 126.7, 126.2, 126.1, 125.9, 125.4, 125.3, 124.8, 123.7, 121.1, 29.8 ppm. HRMS (+ p NSI): Calculated for $\text{C}_{26}\text{H}_{20}\text{SO}$ $[\text{M}+\text{H}]^+$ 381.50934, observed 381.13030.

Procedures for the Density Functional Theory Calculations

All DFT calculations were performed using the Jaguar 9.1 suite of programs.²⁰ Geometry optimization calculations were carried out using Becke's three-parameter exchange functional B3LYP including Grimme's D3 dispersion correction level of theory, with the 6-31G** basis set.²¹⁻²⁶ Rhodium and iridium were represented using the Los Alamos LACVP basis set which includes relativistic core potentials. The energies of the optimized structures were evaluated using single point calculations on the geometry-optimized structures using the same functional (B3LYP-D3) and Dunning's correlation consistent triple- ζ cc-pVTZ(-f) basis set, which includes a double set of polarization functions.²⁷ Analytical vibrational frequencies were calculated according to the harmonic approximation using the 6-31G** basis set in order to confirm proper convergence to well-defined minima or saddle points on the potential energy surface. Solvation energies were calculated according to a self-consistent reaction field (SCRF) approach based on accurate numerical solutions of the Poisson-Boltzmann equation.²⁸⁻³⁰ Solvation energy calculations were performed using the 6-31G**/LACVP basis set with the gas-phase optimized geometry, using a dielectric constant of $\epsilon = 10.36$ for 1,2-dichloroethane (DCE). The calculated solvation energies are subject to empirical parameterization of the atomic radii used to generate the solute surface. Molecular orbital calculations were performed using the M06 functional and Dunning's correlation consistent triple- ζ cc-pVTZ(-f) basis set. The standard set of optimized

radii in Jaguar was used for H (1.150 Å), C (1.900 Å), N (1.600 Å), O (1.600 Å), Cl (1.974 Å), Rh (1.464 Å), and Ir (1.420 Å). Transition states were located with quadratic synchronous transit (QST) search methods.³¹ The Gibbs free energy was calculated as follows:

$$G_{sol} = G_{gas} + G_{solv}$$

$$G_{gas} = H_{gas} - TS_{gas}$$

$$H_{gas} = E(SCF) + ZPE$$

$$\Delta E(SCF) = \Sigma E(SCF)_{products} - \Sigma E(SCF)_{reactants}$$

$$\Delta G_{sol} = \Sigma G_{sol,products} - \Sigma G_{sol,reactants}$$

where G_{sol} is the free energy in solution, G_{gas} is the free energy in the gas phase, G_{solv} is the free energy of solvation calculated according to the continuum solvation model, H_{gas} is the enthalpy in the gas phase, T is the temperature (298.15 K), S_{gas} is the entropy in the gas phase, $E(SCF)$ is the “raw” electronic energy calculated according to the self-consistent field (SCF) procedure, and ZPE is the zero-point energy.

Procedure for the Distortion/Interaction-Activation Fragment Analysis Calculations

The geometry-optimized structures of the metal-dioxazolone complexes were broken into two fragments by removing the metal-nitrogen bond, resulting in an under-coordinated metal complex fragment and a *tert*-butyl dioxazolone fragment. To obtain a “relaxed” energy for each fragment, the energies of the geometry-optimized fragments were then calculated using single point calculations with the B3LYP-D3 functional and Dunning’s correlation consistent triple- ζ cc-pVTZ(-f) basis set. To then determine the distortion energy, the optimized transition state structures for the carbon dioxide removal step that had been previously located using QST search methods as described above were broken into two fragments in the same way as the geometry-

optimized initial structures. The “strained” energy for each fragment was then calculated using the B3LYP-D3 functional and Dunning’s correlation consistent triple- ζ cc-pVTZ(-f) basis set. The distortion/interaction-activation energies depicted in Figures 14 and 15 were then computed as follows:

$$E(SCF)_{distortion} = E(SCF)_{strained} - E(SCF)_{relaxed}$$

$$E(SCF)_{interaction} = \Sigma E(SCF)_{distortion,all\ fragments} - E(SCF)_{transition\ state}$$

where $E(SCF)$ is the “raw” electronic energy calculated for each fragment according to the self-consistent field (SCF) procedure, the subscripts “strained” and “relaxed” refer to the context of the fragment (i.e. “strained” in the transition state or “relaxed” in the initial geometry-optimized structure), the subscript “distortion” refers to the energy caused by physical distortion of the fragment in the transition state, $E(SCF)_{interaction}$ is the stabilization energy caused by the interaction experienced when the fragments are joined together in the transition state and can stabilize each other, and $E(SCF)_{transition\ state}$ specifically refers to the activation energy of the transition state as calculated according to the general procedures described above.

References:

- (1) Afewerki, S.; Cordova, A. Enamine/Transition Metal Combined Catalysis: Catalytic Transformations Involving Organometallic Electrophilic Intermediates. *Topics in Current Chem.* **2019**, *377*, 1-27.
- (2) Harris, R. J.; Park, J.; Nelson, T. A. F.; Iqbal, N.; Salgueiro, D. C.; Bacsa, J.; MacBeth, C. E.; Baik, M.-H.; Blakey, S. B. The Mechanism of Rhodium Catalyzed Allylic C-H Amination. *J. Am. Chem. Soc.* **2020**, *Just Accepted Manuscript*.

- (3) Tsuji, J.; Takahashi, H.; Morikawa, M. Organic syntheses by means of noble metal compounds XVII. Reaction of π -allylpalladium chloride with nucleophiles. *Tet. Lett.* **1965**, *6*, 4387-4388.
- (4) Trost, B. M.; Fullerton, T. J. New synthetic reactions. Allylic alkylation. *J. Am. Chem. Soc.* **1973**, *95*, 292-294.
- (5) Young, A. J.; White, M. C. Catalytic Intermolecular Allylic C-H Alkylation. *J. Am. Chem. Soc.* **2008**, *130*, 14090-14091.
- (6) Cochet, T.; Bellosta, V.; Roche, D.; Ortholand, J.-Y.; Greiner, A.; Cossy, J. Rhodium(III)-catalyzed allylic C-H bond amination. Synthesis of cyclic amines from ω -unsaturated *N*-sulfonylamines. *Chem. Commun.* **2012**, *48*, 10745-10747.
- (7) Shibata, Y.; Kudo, E.; Sugiyama, H.; Uekusa, H.; Tanaka, K. Facile Generation and Isolation of π -Allyl Complexes from Aliphatic Alkenes and an Electron-Deficient Rh(III) Complex: Key Intermediates of Allylic C-H Functionalization. *Organometallics* **2016**, *35*, 1547-1552.
- (8) Burman, J. S.; Blakey, S. B. Regioselective Intermolecular Allylic C-H Amination of Disubstituted Olefins via Rhodium/ π -Allyl Intermediates. *Angew. Chem. Int. Ed.* **2017**, *56*, 13666-13669.
- (9) Nelson, T. A. F.; Blakey, S. B. Intermolecular Allylic C-H Etherification of Internal Olefins. *Angew. Chem. Int. Ed.* **2018**, *57*, 14911-14915.
- (10) Burman, J. S.; Harris, R. J.; Farr, C. M. B.; Bacsa, J.; Blakey, S. B. Rh(III) and Ir(III)Cp* Complexes Provide Complementary Regioselectivity Profiles in Intermolecular Allylic C-H Amidation Reactions. *ACS Catal.* **2019**, *9*, 5474-5479.

- (11) Park, Y.; Heo, J.; Baik, M.-H.; Chang, S. Why is the Ir(III)-Mediated Amido Transfer Reaction Much Faster Than the Rh(III)-Mediated Reaction? A Combined Experimental and Computational Study. *J. Am. Chem. Soc.* **2016**, *138*, 14020-14029.
- (12) Trost, B. M.; Ryan, M. C. Indenylmetal Catalysis in Organic Synthesis. *Angew. Chem. Int. Ed.* **2017**, *56*, 2862-2879.
- (13) Trost, B. M.; Ryan, M. C.; Maurer, D. Development of a Coordinatively Unsaturated Chiral Indenylruthenium Catalyst. *Org. Lett.* **2016**, *18*, 3166-3169.
- (14) Negishi, E.; Tan, Z.; Liang, B.; Novak, T. An efficient and general route to reduced polypropionates via Zr-catalyzed asymmetric CC bond formation. *Proc. Natl. Acad. Sci. U. S. A.* **2004**, *101*, 5782-5787.
- (15) Gutnov, A.; Heller, B.; Fischer, C.; Drexler, H.-J.; Spannenberg, A.; Sundermann, B.; Sundermann, C. Cobalt(I)-Catalyzed Asymmetric [2+2+2] Cycloaddition of Alkynes and Nitriles: Synthesis of Enantiomerically Enriched Atropoisomers of 2-Arylpyridines. *Angew. Chem. Int. Ed.* **2004**, *43*, 3795-3797.
- (16) Farr, C. M. B.; Blakey, S. B. Emory University, Atlanta, GA. Unpublished work, 2019.
- (17) Baker, R. W.; Radzey, H.; Lucas, N. T.; Turner, P. Stereospecific Syntheses and Structures of Planar Chiral Bidentate η^5 : κ S-Indenyl-Sulfanyl and -Sulfinyl Complexes of Rhodium(III). *Organometallics* **2012**, *31*, 5622-5633.
- (18) Park, J.; Baik, M.-H. Korea Advanced Institute of Science and Technology, Daejeon, Republic of Korea. Unpublished work, 2019.

- (19) Bickelhaupt, F. M.; Houk, K. N. Analyzing Reaction Rates with the Distortion/Interaction-Activation Strain Model. *Angew. Chem. Int. Ed.* **2017**, *56*, 10070-10086.
- (20) Bochevarov, A. D.; Harder, E.; Hughes, T. F.; Greenwood, J. R.; Braden, D. A.; Philipp, D. M.; Rinaldo, D.; Halls, M. D.; Zhang, J.; Friesner, R. Jaguar: A high-performance quantum chemistry software program with strengths in life and materials sciences. *Int. J. Quantum Chem.* **2013**, *113*, 2110-2142.
- (21) Slater, J. C. Quantum Theory of Molecules and Solids, Vol. 4: The Self-Consistent Field for Molecules and Solids. McGraw-Hill: New York, **1974**.
- (22) Vosko, S. H.; Wilk, L.; Nusair, M. Accurate spin-dependent electron liquid correlation energies for local spin density calculations: a critical analysis. *Can. J. Phys.* **1980**, *58*, 1200-1211.
- (23) Becke, A. D. Density-functional exchange-energy approximation with correct asymptotic behavior. *Phys. Rev. A* **1988**, *38*, 3098-3100.
- (24) Lee, C.; Yang, W.; Parr, R. G. Development of the Colle-Salvetti correlation-energy formula into a functional of the electron density. *Phys. Rev. B* **1988**, *37*, 785-789.
- (25) Becke, A. D. Density-functional thermochemistry. III. The role of exact exchange. *J. Chem. Phys.* **1993**, *98*, 5648-5652.
- (26) Grimme, S.; Antony, J.; Ehrlich, S.; Krieg, S. A consistent and accurate ab initio parameterization of density functional dispersion correction (DFT-D) for the 94 elements H-Pu. *J. Chem. Phys.* **2010**, *132*, 154104.
- (27) Dunning, T. H. Gaussian basis sets for use in correlated molecular calculations. I. The atoms boron through neon and hydrogen. *J. Chem. Phys.* **1989**, *90*, 1007-1023.

- (28) Marten, B.; Kim, K.; Cortis, C.; Friesner, R. A.; Murphy, R. B.; Ringnalda, M. N.; Sitkoff, D.; Honig, B. New Model for Calculation of Solvation Free Energies: Correction of Self-Consistent Reaction Field Continuum Dielectric Theory for Short-Range Hydrogen-Bonding Effects. *J. Phys. Chem.* **1996**, *100*, 11775-11788.
- (29) Friedrichs, M.; Zhou, R. H.; Edinger, S. R.; Friesner, R. A. Poisson-Boltzmann Analytical Gradients for Molecular Modeling Calculations. *J. Phys. Chem. B* **1999**, *103*, 3057-3061.
- (30) Edinger, S. R.; Cortis, C.; Shenkin, P. S.; Friesner, R. A. Solvation Free Energies of Peptides: Comparison of Approximate Continuum Solvation Models with Accurate Solution of the Poisson-Boltzmann Equation. *J. Phys. Chem. B* **1997**, *101*, 1190-1197.
- (31) Peng, C.; Schlegel, H. B. Combining Synchronous Transit and Quasi-Newton Methods to Find Transition States. *Isr. J. Chem.* **1993**, *33*, 449-454.